Molecular Structure, Optical, and Magnetic Properties of Free-Base Naphthalocyanine Dianions

AUTHOR(S):

Konarev, Dmitri V.; Khasanov, Salavat S.; Nakano, Yoshiaki; Shestakov, Alexander F.; Ishikawa, Manabu; Otsuka, Akihiro; Yamochi, Hideki; Kitagawa, Hiroshi; Lyubovskaya, Rimma N.

CITATION:

Konarev, Dmitri V. ...[et al]. Molecular Structure, Optical, and Magnetic Properties of Free-Base Naphthalocyanine Dianions. European Journal of Organic Chemistry 2018, 2018(26): 3410-3415

ISSUE DATE:

2018-07-13

URL:

http://hdl.handle.net/2433/232622

Molecular Structure, Optical and Magnetic Properties of Free-Base Naphthalocyanine H_2Nc^{2-} Dianions.

Dmitri V. Konarev,*[a] Salavat S. Khasanov,[b] Yoshiaki Nakano,[c, d] Alexander F. Shestakov,[a] Manabu Ishikawa,[c, d] Akihiro Otsuka,[c, d] Hideki Yamochi,[c, d] Hiroshi Kitagawa,[c] and Rimma N. Lyubovskaya[a]

Abstract: Reduction of free-base naphthalocyanine (H_2Nc) with sodium fluorenone ketyl and an excess of (PPN^+)(Cl^-), where PPN^+ is bis(triphenylphosphoranylidene)ammonium cation, unexpectedly allows the synthesis of the $(PPN^+)_2(H_2Nc^{2-})$ salt (**1**). Since sodium fluorenone ketyl can generate only $H_2Nc^{\bullet-}$ radical anions, the formation of H_2Nc^{2-} is realized most probably due to disproportionation of $H_2Nc^{\bullet-}$ to H_2Nc^0 and H_2Nc^{2-}. The H_2Nc^{2-} dianions form layers in **1** in which π-π stacks of H_2Nc^{2-} are formed along the *a* direction with a short interplanar distance of 3.30 Å and a HOMO-HOMO overlap integral of 3.1×10^{-3}. The H_2Nc^{2-} macrocycle shows essential distortion due to the formation of oppositely located short and long C-N(imine) bonds. Distortion of the macrocycle increases with the negative charge on H_2Nc due to occupation of the lowest unoccupied (LU) orbital. According to the calculations, distortion disappears in a triplet state of H_2Nc^{2-} due to the occupation of both LU and LU+1 orbitals which averages their effect on geometry of the macrocycle. Optical spectrum of **1** shows the lowest energy absorption band at 1230 nm attributed to the HO → LU+1 excitation and a blue shift of the Q-band of H_2Nc. Salt **1** is EPR silent indicating diamagnetic singlet state of the H_2Nc^{2-} dianions. According to the DFT calculations open shell broken symmetry singlet state is lower in energy than the corresponding closed shell singlet and triplet states. Large singlet−triplet energy gap indicates that the corresponding triplet state is thermally inaccessible.

Introduction

Organic macroheterocycles are effective building blocks for preparation of complexes with various metal ions. These complexes together with pristine macroheterocycles attract essential interest as materials with promising optical and conducting properties as well as molecular components for supramolecular assemblies.[1] Compounds possessing conductivity or magnetism are obtained by oxidation of pristine free-base or metal-containing phthalocyanines (MPc) by iodine or electrochemical oxidation of the $[M^{III}(CN)_2Pc]^-$ anions in the presence of organic cations. Metallic conductivity is realized in some compounds with partially oxidized macrocycles having the columnar or layered arrangement.[1c, 2] Compounds with ferrimagnetic ordering of spins were obtained at the oxidation of manganese(II) phthalocyanine by tetracyanoethylene.[3] Reduction of organic macroheterocycles is studied less thoroughly. Recently a series of salts of free-base phthalocyanine radical anions ($H_2Pc^{\bullet-}$) with different cations was obtained allowing one to study the effect of reduction on molecular structure, optical and magnetic properties of H_2Pc.[4] Free-base triphenylcorrole (H_3TPCor) was reduced to the radical anion state and the reduction was shown to be accompanied by deprotonation to form paramagnetic radical $H_2TPCor^{\bullet2-}$ dianions.[5] Radical anions of free-base tetra(4-pyridyl) porphyrin were also studied in solid state.[6] The macrocycle with extended π-system, naphthalocyanine (Nc, scheme 1), the first and second reduction potentials of -0.97~ -1.15 and -1.35~ -1.55 V *vs* SCE, respectively, in complexes with silicon and zinc.[7] The strength as an acceptor is intermediate between those of free-base phthalocyanine (E_{red} = -0.66 V *vs* SCE) and free-base substituted porphyrins (-1.23~ -1.46 V *vs* SCE).[8] These data show that the $H_2Nc^{\bullet-}$ radical anions can be obtained when treated with relatively strong reductants such as sodium fluorenone ketyl (E_{ox} = -1.3 V)[9] but the H_2Nc^{2-} dianions are not available with this reductant because of the very negative second reduction potential. This is the general reason why dianions of free-base organic macroheterocycles have not been obtained yet in solid state though some of them can be generated electrochemically in solution.[8,10]

Scheme 1

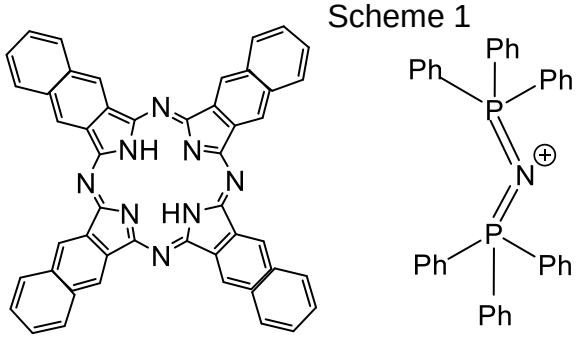

In this work we present for the first time solid state structure and properties of free-base naphthalocyanine dianion (H_2Nc^{2-}). These dianions are obtained in the crystalline salt with bis(triphenylphosphoranylidene)ammonium cations (Scheme 1): $(PPN^+)_2(H_2Nc^{2-})$ (**1**). Reduction allows one to dissolve initially insoluble free-base naphthalocyanine, prepare single crystals and study their crystal structure, optical and magnetic properties. While the synthesis, solid state structure and properties of doubly reduced macroheterocycles have been absent, here we present these data for the first time. DFT

[a] Dr. D.V. Konarev, Prof. R. N. Lyubovskaya,Prof. A. F. Shestakov
Institute of Problems of Chemical Physics RAS, Chernogolovka, Moscow region, 142432 Russia, konarev3@yandex.ru.
[b] Dr. S.S. Khasanov
Institute of Solid State Physics RAS, Chernogolovka, Moscow region, 142432 Russia.
[c] Division of Chemistry, Graduate School of Science, Kyoto University, Sakyo-ku, Kyoto 606-8502, Japan;
[d] Research Center for Low Temperature and Materials Sciences, Kyoto University, Sakyo-ku, Kyoto 606-8501, Japan
Supporting information for this article is given via a link at the end of the document.

calculations elucidate the nature of distortion, the electronic structure and magnetic behavior of negatively charged Nc macrocycle.

Results and discussion

Synthesis.

For the synthesis of $(PPN^+)_2(H_2Nc^{2-})$ (**1**), the general strategy to reduce free-base and metal-containing phthalocyanines was applied which utilizes an excess of sodium fluorenone ketyl in the presence of an excess of organic cations.[4b] In case of free-base naphthalocyanine (H_2Nc), the synthesis was carried out with 2.4 equivalents of sodium fluorenone ketyl and more than a 3-fold molar excess of $(PPN^+)(Cl^-)$. Previously, it was shown that titanyl naphthalocyanine $[Ti^{IV}O(Nc^{2-})]^0$ is reduced in these conditions to the $[Ti^{IV}O(Nc^{\bullet 3-})]^{\bullet -}$ radical anions only.[10] Similarly, free-base phthalocyanine (H_2Pc) being a stronger acceptor than naphthalocyanine forms $H_2Pc^{\bullet -}$ radical anions when an excess of reductant and cations is used.[4b] Therefore, we expected the formation of the $H_2Nc^{\bullet -}$ radical anions in these conditions. H_2Nc is completely dissolved at the reduction forming deep green solution. Slow mixing of the obtained solution with *n*-hexane during month yields small square prisms of black color (**1**) and large amount of green powder. Prisms were separated from the powder under microscope in the glovebox (the yield of crystals was about 12%). According to the IR and visible-NIR spectra, green powder obtained in the synthesis of **1** is starting H_2Nc. Since neutral H_2Nc is not soluble in *o*-dichlorobenzene, we supposed that it is formed during the precipitation of crystals of **1** as a result of the disproportionation of $H_2Nc^{\bullet -}$ to give neutral H_2Nc and dianionic H_2Nc^{2-}. Thus, though the H_2Nc^{2-} dianions cannot be directly obtained at the reduction with sodium fluorenone ketyl, they are formed in the disproportionation reaction. This mechanism should allow the formation of highly reduced states of other macroheterocycles having very negative reduction potential. The black crystals were studied by X-ray diffraction, IR, UV-vis-NIR and EPR spectroscopy. The composition of **1** was determined from X-ray diffraction analysis on a single crystal to be $(PPN^+)_2(H_2Nc^{2-})$ (**1**). Several crystals from one synthesis belong to one crystalline phase. Elemental analysis could not be used to confirm the composition of **1** due to extremely high air-sensitivity.

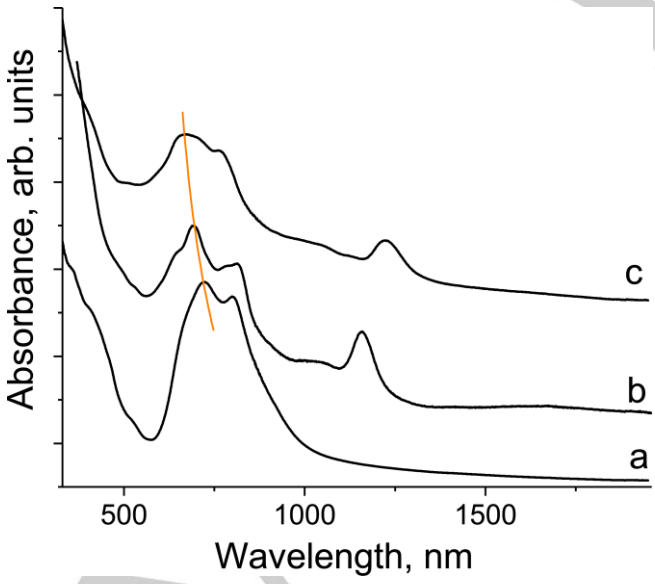

Figure 1. Spectra of: (a) pristine free-base naphthalocyanine (H_2Nc); (b) salt $(PPN^+)[Ti^{IV}O(Nc^{\bullet 3-})]^{\bullet -}$ containing deprotonated $Nc^{\bullet 3-}$ radical trianions according to Ref. [11] and (c) salt **1** in the UV-visible-NIR range measured in KBr pellets prepared in anaerobic conditions.

Optical spectra.

Pristine free-base H_2Nc has intense absorption in the visible range. The Q-band observed in the spectrum is split at 724 and 800 nm (Fig. 1a). Spectrum of **1** was measured for several single crystals selected carefully under microscope (Fig. 1c). The formation of **1** is accompanied by a noticeable blue shift of the spilt Q-band to 674 and 768 nm. A new band is also manifested in the spectrum of **1** in the NIR range with maximum at 1230 nm (Fig. 1c) indicating that the H_2Nc^{2-} dianions have the lowest energy transition at about 1 eV. It should be noted that the previously studied titanyl naphthalocyanine radical trianions in $(PPN^+)[Ti^{IV}O(Nc^{\bullet 3-})]^{\bullet -}$ showed the lowest energy absorption band of similar intensity at 1160 nm (Fig. 1b).[11] Therefore, we suppose that the absorption band at 1230 nm in the spectrum of **1** can be attributed to the H_2Nc^{2-} dianions but not originated from $H_2Nc^{\bullet -}$ which can be generated in the sample due to oxidation of H_2Nc^{2-}. Also, according to EPR measurements, the content of paramagnetic species was less than 4.6% that is too small to provide the intense band in NIR range.

Crystal structure.

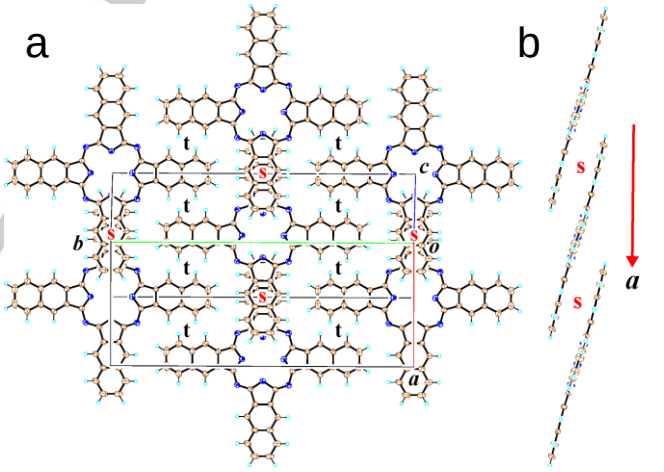

Figure 2. (a) View on the layers composed of H_2Nc^{2-} dianions in **1**; (b) view on the π-stacking chain of H_2Nc^{2-}dianions arranged along the *a*-axis. Hydrogen atoms in the center of the macrocycles and the PPN^+ cations are not shown.

Crystal structure of **1** was solved at 250 K.‡ It contained half of independent H_2Nc^{2-} and two halves of independent PPN^+ cations. Naphthalocyanine layers arranged in the *ab* plane alternate with the cationic PPN^+ layers in the structure of **1** (Figs. 2 and S2). There are two types of π-π interaction between H_2Nc^{2-} in the layers. Strong π-π interaction is realized along the *a* axis due to the overlapping of π-orbitals on naphthalene fragments of H_2Nc^{2-} arranged parallel to each other (the dihedral angle between them is only 0.58°) with a short interplanar distance of 3.30 Å. As a result, effective uniform stacking is

attained along the *a* axis with overlap integral of 3.1×10^{-3} (the overlap integral **s** in Fig. 2a was calculated by the extended Hückel method)[12]. Contrary, the overlap between the naphthalene fragments of H_2Nc^{2-} between the neighboring stacks along the *a* axis is very weak (the overlap integral **t** in Fig. 2 is only 0.1×10^{-3}).

The crystal structure of pristine H_2Nc is unknown while that of H_2Pc was studied. In free-base H_2Pc there are two types of the C-N bonds differing in length in the macrocycle with the pyrrole and imine nitrogen atoms. No alternation of each types bonds is observed in pristine H_2Pc.[13] Alternation of the C-N(imine) and C-C(meso) bonds was, however, found for negatively charged free-base phthalocyanine, corrole and porphyrin macrocycles.[4, 5, 6] The average length of the C-N(pyrrole) bonds in the H_2Nc^{2-} dianions is 1.379(13) Å. At the same time there are short and long C-N(imine) bonds in the H_2Nc^{2-} macrocycle with the length of 1.300(12) and 1.367(12) Å. It is interesting that the difference between the short and long bonds observed for H_2Nc^{2-} (0.067 Å) essentially exceeds such difference for the $Nc^{\bullet3-}$ radical trianions in $[Ti^{IV}O(Nc^{\bullet3-})]^{\bullet-}$ (0.038 Å)[11]. Therefore, the increment of change is regarded to enhance the distortion.

Magnetic properties.

Magnetic properties of **1** were studied by EPR technique on several carefully selected single crystals. The salt shows a weak very narrow Lorentzian EPR signal with $g = 2.0034$ and linewidth of 0.141 mT at room temperature. The temperature dependence of signal intensity is pure paramagnetic down to 4 K with Weiss temperature close to 0 K. Since parameters of the signal are very close to those in the salts with the $H_2Pc^{\bullet-}$ radical anions,[4a, 4c] it can be attributed to small amount of the $H_2Nc^{\bullet-}$ impurity in the sample. As it was estimated from integral intensity of the signal the content of $H_2Nc^{\bullet-}$ is less than 4.6% from the total amount of free base naphthalocyanine. We suppose that relatively high content of paramagnetic impurity is due to the very high oxygen sensitivity of the H_2Nc^{2-} dianions concerning the negative second reduction potential of H_2Nc (-1.23~ -1.46 V)[7]. Thus, the H_2Nc^{2-} dianion is assigned to be an EPR silent species and have diamagnetic singlet ground state.

Theoretical calculations.

DFT calculations based on PBE functional were made for H_2Nc in neutral, radical anion and dianion (singlet ground and triplet excited) states (Figs. S3-S6). For all species the optimized geometry has exact D_{2h} symmetry or small deviation due to C_{2h} distortion within 0.0001 - 0.0003 Å in bond lengths for the $H_2Nc^{\bullet-}$ radical anion and H_2Nc^{2-} dianion in singlet state. DFT calculations for pristine H_2Nc yielded small distortion of the macrocycle since in this case the difference between short and long bonds is only 0.020 Å (Fig. S3). This difference increases at the change to the radical anion (0.042 Å) and finally to the dianion state (0.058 Å) (Figs. S4 and S5). It should be noted that the difference calculated for the dianion is close to the experimentally determined value of 0.067 Å. The distortion of H_2Nc is developed with the shortening of four C-N(imine) bonds from the initial length of 1.321 Å on 0.008 and 0.013 Å and with the elongation of four C-N(imine) bonds from the initial length of 1.341 Å on 0.014 Å and 0.025 Å at an addition of one and two electrons, respectively, to the macrocycle. The reason is that the lowest unoccupied (LU) orbital of H_2Nc is bonding and antibonding for the shortened and elongated C-N(imine) bonds. Therefore, the distortion increases by a factor of two at the double LU orbital population in H_2Nc^{2-} with respect to $H_2Nc^{\bullet-}$. At the same time according to the calculations, the distortions for the H_2Nc^{2-} dianions in triplet excited state (0.014 Å) are of the same order as in pristine H_2Nc (0.020 Å). The LU+1 orbital of b_{2g} symmetry has a similar structure to that of the LU orbital of b_{1g} symmetry but it is rotated relative to the LU orbital at an angle of 90° about the C_2 axis located perpendicular to the macrocycle plane. Thus, the population of the LU+1 orbital has an opposite effect on the same C-N(imine) bonds. As a result, positive and

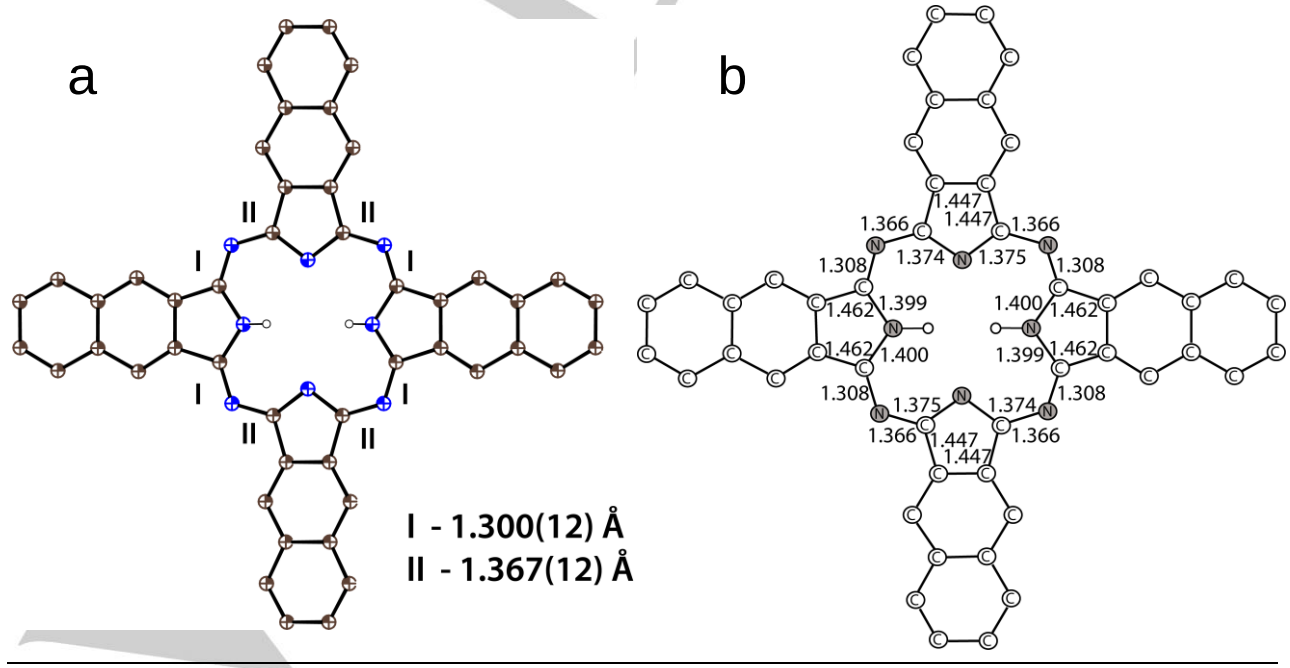

Figure 3. Molecular structure of: (a) the H_2Nc^{2-} dianions in salt **1** according to the X-ray diffraction analysis. Short and long C-N(imine) bonds are marked as I and II, respectively; (b) optimized structure of the H_2Nc^{2-} dianions in singlet ground state according to the DFT calculations.

negative effects are roughly cancelled and strong alteration of C-N(imine) bonds disappears in the triplet state of H_2Nc^{2-}.

To gain further insight into the electronic structure of H_2Nc^{2-}, theoretical analyses were performed at the CAM-B3LYP and M11/cc-pVDZ levels of theory, where partial geometry optimization on the hydrogen atoms only from the X-ray structure with C_2 symmetry and full geometry optimization with D_{2h} symmetry were carried out. For comparison, oligoacenes were also analysed at the same levels of theory. The results for H_2Pc^{2-} and oligoacenes are summarized in Table S4. In the case of partial optimization, both CAM-B3LYP and M11 functionals indicate that the open-shell broken symmetry singlet state is lower in energy than the corresponding closed-shell singlet and triplet states, whereas the PBE functional predicts the ground state is of closed-shell singlet. The CAM-B3LYP and M11 functionals indicate large singlet−triplet gaps of 5729 and 7176 K, respectively, indicating that the triplet state is thermally inaccessible in accordance with the EPR data. In the case of full optimization, the CAM-B3LYP functional predicts that the ground state is a broken symmetry singlet, whereas the M11 functional does not predict the broken symmetry singlet state. It should be noted that the $^3B_2$ state of C_{2v}-symmetric H_2Nc^{2-} rather than the $^3B_{3g}$ state of D_{2h}-symmetric H_2Nc^{2-} is located at the local minimum. The non-spin-projected and spin-projected diradical characters y_i and y_i^{SP} (i = 0 and 1) were estimated from the occupation numbers of paired natural orbitals n(HO−i) and n(LU+i)[14], where HO and LU correspond to HOMO and LUMO of H_2Nc^{2-} dianion state, respectively:

$$y_i = n(\mathrm{LU}+i) = 2 - n(\mathrm{HO}-i) \quad (1)$$

$$y_i^{SP} = n^{SP}(\mathrm{LU}+i) = 2 - n^{SP}(\mathrm{HO}-i) = [n(\mathrm{LU}+i)]^2/(1 + S_i^2) = 2 - [n(\mathrm{HO}-i)]^2/(1 + S_i^2) \quad (2)$$

$$S_i = [n(\mathrm{HO}-i) - n(\mathrm{LU}+i)]/2 \quad (3)$$

The $y_0^{(SP)}$ and $y_1^{(SP)}$ values are indices of the diradical and tetraradical, respectively, e.g., $y_0^{(SP)} = y_1^{(SP)} = 0$ (closed-shell); $y_0^{(SP)} = 1$, $y_1^{(SP)} = 0$ (pure diradical); $y_0^{(SP)} = y_1^{(SP)} = 1$ (pure tetraradical). $y_1^{(SP)}$ of H_2Nc^{2-} is also almost zero and $y_0^{(SP)}$ is finite, indicating that H_2Nc^{2-} is a singlet diradicaloid, the diradical character of which is positioned between those of pentacene and hexacene (Tables 1 and S5).

Table 1. Non-spin-projected and spin-projected diradical characters, y_i and y_i^{SP} (i = 0 and 1), for the open-shell broken-symmetry singlet states of H_2Nc^{2-} and oligoacenes calculated at the CAM-B3LYP and M11/cc-pVDZ level of theory.

	$(H_2Nc^{2-})^a$	$(H_2Nc^{2-})^b$	Penta-cene	Hexa-cene	Hepta-cene	Octa-cene
CAM-B3LYP						
y_0	0.291	0.209	0.118	0.407	0.589	0.708
y_1	0.035	0.025	0.014	0.055	0.097	0.147
y_0^{SP}	0.056	0.027	0.008	0.123	0.296	0.462
y_1^{SP}	0.001	0.000	0.000	0.002	0.005	0.012
M11						
y_0	0.254	0.000	0.041	0.391	0.577	0.692
y_1	0.036	0.000	0.005	0.057	0.102	0.154
y_0^{SP}	0.041	0.000	0.001	0.112	0.283	0.437
y_1^{SP}	0.001	0.000	0.000	0.002	0.006	0.014

[a] Only coordinates of hydrogen atoms were optimized from X-ray structure. [b] Full optimization was done in the D_{2h} symmetry.

The energy diagrams for the frontier Kohn−Sham orbitals of the broken symmetry states in C_2-symmetric H_2Nc^{2-} calculated at the CAM-B3LYP and M11/cc-pVDZ level of theory are shown in Figs. S9 and S10, respectively. Both functionals afford the similar results, and the highest occupied (HO) and LU orbitals mainly spread over the unprotonated and protonated benzoisoindole moieties, respectively. As a result, the unprotonated benzoisoindole moiety is more negatively charged (Figs. S11 and S12). Based on the time-dependent density functional theory (TD-DFT) at the same levels of theory, the calculated excitation energies, oscillator strengths, $\langle S^2 \rangle$ values, and assignments on the low-lying excited states of C_2-symmetric H_2Nc^{2-} are summarized in Tables S6 and S7. The observed and calculated UV-vis-NIR spectra are compared in Fig. 4. Fig. 4 also shows the UV-vis-NIR spectra calculated on the base of PBE functional for C_{2h}-symmetric H_2Nc^{2-} in the closed shell singlet ^1A_g state as well.

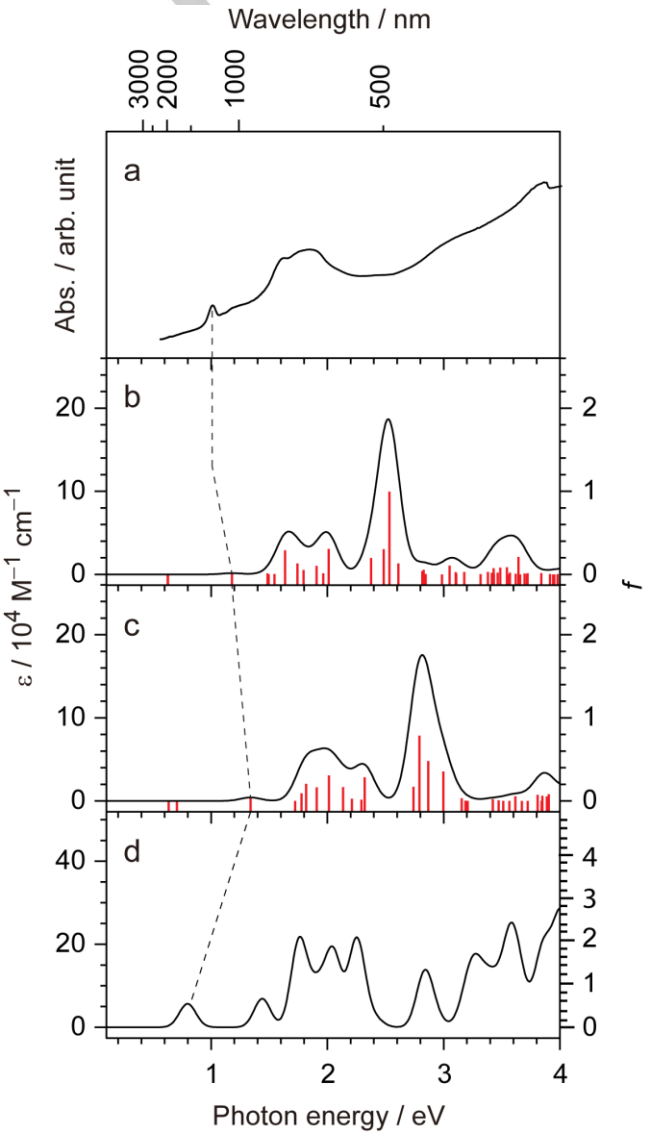

Figure 4. (a) Observed UV-vis-NIR spectrum of $(PPN)_2H_2Nc$ in KBr. Theoretical spectra of the broken symmetry singlet states in C_2-symmetric H_2Nc^{2-} by (b) CAM-B3LYP and (c) M11 functionals and closed shell singlet state in D_{2h}-symmetric H_2Nc^{2-} by PBE functional (d).

All functionals predict that lowest excitations of HO → LU character at an energy below 0.71 eV are forbidden transitions. The first observable transition mainly have the character of HO → LU+1 excitation, and the excitation energies are 1.179 eV, 1.339 eV and 0.793 eV by CAM-B3LYP, M11 and PBE, respectively (Fig. 4). Therefore, the observed absorption band at 1.01 eV (1230 nm) can be tentatively assigned as the third excited state with the character of HO → LU+1 excitation.

Open-shell singlet diradicaloid state when frontier orbitals are distributed in different spaces of molecule producing unpaired spin density is a very interesting phenomenon. Such molecules have rather small HOMO−LUMO energy gap, and can show high conductivity of semiconducting type and temperature induced EPR signals.[15] Generally π-extended aromatic hydrocarbon molecules (polyacenes, biphenalenes, anthenes, and zenthrenes)[15] manifest such states. At the same time open shell singlet diradicaloid state is rare for macroheterocycles, which have large π-electron system.[16] Among them nickel(II) and copper(II) corroles are diradicals,[16a, 16b] and doubly linked oxidized corrole dimer and its zinc(II) complex also show singlet diradical character.[16c]

Conclusion

Thus, reduction of H_2Nc by an excess of sodium fluorenone ketyl in the presence of $(PPN^+)(Cl^-)$ followed by precipitation of crystals by *n*-hexane yields $(PPN^+)_2(H_2Nc^{2-})$ (**1**). This salt presents a first example of free-base macroheterocycle dianion obtained and characterized in solid state. Since these dianions can be obtained only at very negative reduction potentials, we suppose that the main route for the formation of **1** is disproportionation of $H_2Nc^{\bullet-}$ to neutral H_2Nc and dianion H_2Nc^{2-}. This method of preparation can provide highly reduced species of macroheterocycles. Essential distortion of the H_2Nc^{2-} macrocycle is shown. It is explained by the population of the LU orbital which is bonding for the shortened bonds and antibonding for the elongated bonds. This distortion is averaged in a triplet excited state of H_2Nc^{2-}. Spectrum of **1** has the lowest energy absorption band at 1230 nm attributed to the HO → LU+1 excitation. Salt **1** is in a diamagnetic singlet state. In accordance with the DFT calculations open shell broken symmetry singlet state is the lowest state in energy, whereas singlet−triplet gap is rather large in the H_2Nc^{2-} dianion indicating inaccessibility of triplet state at room temperature. Our work shows that naphthalocyanine dianions manifest the sign of diradicaloid character. The search for other macroheterocycles of such type is in progress.

Experimental Section

Materials.

Metal-free naphthalocyanine (H_2Nc, >95%), bis(triphenylphosphoranylidene)ammonium chloride (PPNCl, >97%) was purchased from Aldrich. Sodium fluorenone ketyl was obtained according to Ref. [17]. *o*-Dichlorobenzene ($C_6H_4Cl_2$, Acros) was distilled over CaH_2 under reduced pressure and *n*-hexane was distilled over Na/benzophenone. Solvents were degassed and stored in an MBraun 150B-G glove box. Salt **1** was synthesized and stored in a glove box with controlled atmosphere containing less than 1 ppm of water and oxygen. KBr pellets used for the IR and UV-visible-NIR analyses were prepared in the glove box. EPR measurements were performed on polycrystalline sample of **1** sealed in 2 mm quarz tube under ambient pressure.

General.

UV-visible-NIR spectra were measured in KBr pellets on a PerkinElmer Lambda 1050 spectrometer in the 250-2500 nm range. FT-IR spectra were obtained in KBr pellets with a PerkinElmer Spectrum 400 spectrometer (400-7800 cm^{-1}). EPR spectra of **1** were recorded for polycrystalline sample with a JEOL JES-TE 200 X-band ESR spectrometer equipped with a JEOL ES-CT470 cryostat between room temperature and 4.1 K.

Synthesis.

Crystals of $(PPN^+)_2(H_2Nc^{2-})$ (**1**) were obtained by diffusion technique. H_2Nc (29.8 mg, 0.042 mmol) was reduced by 2.4 equivalents of sodium fluorenone ketyl (20,3 mg, 0.101 mmol) in the presence of three equivalent of PPNCl (71.8 mg, 0.126 mmol) in 16 mL of *o*-dichlorobenzene by stirring at 80°C during 24 hours. H_2Nc completely dissolved to form deep green solution which was cooled down to room temperature and filtered into a 1.8-cm-diameter, 50 mL glass tube with a ground glass plug, and then 30 mL of *n*-hexane was layered over the solution. Slow mixing of the solutions resulted in precipitation of crystals and large amount of green powder over 1 month. The solvent was then decanted and precipitate was washed with *n*-hexane. Crystals were separated from the powder under microscope in the glovebox According to the IR and visible-NIR spectra, green powder obtained in the synthesis of **1** was starting H_2Nc. The composition of **1** was determined from X-ray diffraction analysis on a single crystal to be $(PPN^+)_2(H_2Nc^{2-})$ (**1**). Several crystals from one synthesis belong to one crystalline phase. Elemental analysis could not be used to confirm the composition of **1** due to extremely high air-sensitivity. Small square prisms of **1** have black color and were obtained with the yield of 12%.

X-ray crystal structure determination.

Crystal data for **1** at 100(1) K: $C_{120}H_{86}N_{10}P_4$, M_r = 1791.86 g mol^{-1}, black prism, monoclinic, *C*2, *a* = 12.0654(6), *b* = 28.2519(12), *c* = 13.9880(6) Å, β = 100.028(2)°, *V* = 4695.3(4) $Å^3$, *Z* = 2, d_{calc} = 1.267 g·cm^{-3}, μ = 0.139 mm^{-1}, *F*(000) = 1872, $2\theta_{max}$ = 50.484°, reflections measured 9377, unique reflections 4913, reflections with $I > 2\sigma(I)$ = 3328, parameters refined 625, restraints 699, R_1 = 0.0627, wR_2 = 0.1522, G.O.F. = 1.032, CCDC 1825619.

X-ray diffraction data for **1** were collected on a Bruker Smart Apex II CCD diffractometer with graphite monochromated MoK_α radiation using a Japan Thermal Engineering Co. cooling system DX-CS190LD. Raw data reduction to F^2 was performed using a Bruker SAINT.[18] The structure was solved by direct method and refined by the full-matrix least-squares method against F^2 using SHELX-2013.[19] Non-hydrogen atoms were refined anisotropically. Positions of hydrogen atoms were calculated geometrically. Two of six phenyl substituents of one PPN^+ cation are rotationally disordered between two orientations with the 0.63(3)/0.37(3) and 0.58(4)/0.42(4) occupancies. To keep the anisotropic thermal parameters of the disordered parts within the reasonable limits the displacement components were restrained using ISOR, SIMU and DELU SHELXL instructions. That resulted in 699 restraints used for the refinement of the crystal structure of **1**.

Acknowledgements

The work was supported by Russian Science Foundation grant № 17-13-01215, and by a Grant-in-Aid for Scientific Research on Innovative Areas, ‘‘π-System Figuration: Control of Electron and Structural Dynamism for Innovative Functions,’’ from the Japan Society for the Promotion of Science (JSPS) JP17H05153, and by JSPS KAKENHI Grant Numbers JP15K17901 and JP26288035, and the

JST (ACCEL) 27 (100150500010) project. The computations were partly performed using the Research Center for Computational Science, Okazaki, Japan.

Keywords: free-base naphthalocyanine dianions, reduction, crystal structure, IR, UV-visible-NIR spectra, DFT calculations.

Conflict of interest

The authors declare no conflict of interest.

[1] (*a*) T. Nyokong, *Coord. Chem. Rev.*, **2007**, *251*, 1707–1722; (*b*) C. G. Claessens, W. J. Blau, M. Cook, M. Hanack, R. J. M. Nolte, T. Torres, D. Wöhrle, *Monat. Chem.*, **2001**, *132*, 3–11; (c) T. Inabe, H. Tajima, *Chem. Rev*. **2004**, *104*, 5503–5534; (d) I. Beletskaya, V. S. Tyurin, A. Y. Tsivadze, R. Guilard, C. Stern, *Chem. Rev.*, **2009**, *109*, 1659–1713..

[2] (a) J. L. Petersen, C. S. Schramm, D. R. Stojakovic, B. M. Hoffman, T. J. Marks, *J. Am. Chem. Soc*. **1977**, *99*, 286–288; (b) H. Hasegawa, T. Naito, T. Inabe, T. Akutagawa, T. Nakamura, *J. Mater. Chem*. **1998**, *8*, 1567–1570; (c) M. Matsuda, T. Naito, T. Inabe, N. Hanasaki, H. Tajima, T. Otsuka, K. Awaga, B. Narymbetov, H. Kobayashi, *J. Mater.Chem.* **2000**, *10*, 631–636..

[3] D. K. Rittenberg, L. Baars-Hibbe, A. B. Böhm, J. S. Miller, *J. Mater. Chem.* **2000**, *10*, 241–244.

[4] a). D. V. Konarev, L. V. Zorina, S. S. Khasanov, A. L. Litvinov, A. Otsuka, H. Yamochi, G. Saito, R. N. Lyubovskaya, *Dalton Trans.,* **2013**, *42*, 6810–6816; b) D. V. Konarev, A. V. Kuzmin, M. A. Faraonov, M. Ishikawa, Y. Nakano, S. S. Khasanov, A. Otsuka, H. Yamochi, G. Saito, R.N. Lyubovskaya, *Chem. Eur. J.* **2015**, *21*, 1014–1028; (c) D. V. Konarev, S. S. Khasanov, M. Ishikawa, A. Otsuka, H. Yamochi, G. Saito, R.N. Lyubovskaya, *Dalton Trans.,* **2017**, *46*, 3492–3499.

[5] D.V. Konarev, D.R. Karimov, S.S. Khasanov, A. Otsuka, H. Yamochi, H. Kitagawa, R.N. Lyubovskaya, *Dalton. Trans*., **2017**, *46*, 13994–14001.

[6] D.V. Konarev, A. V. Kuzmin, S. S. Khasanov, A. Otsuka. H. Yamochi, H. Kitagawa, R. N. Lyubovskaya, *J. Org. Chem*., **2018,** *83*, 1861–1866.

[7] (a) V. Novakova, P. Reimerova, J. Svec, D. Suchan, M. Miletin, H. M. Rhoda, V. N. Nemykin, P. Zimcik, *Dalton Trans.*, **2015**, *44*, 13220–13233; (b) B. L. Wheeler, G. Nagasubramanian, J. Bard, L. A. Schechtman, D. R. Dininny, M. E. Kenney, *J. Am. Chem. Soc*., **1984**, *106*, 7404–7410.

[8] (a) A. B. P. Lever, *Inorg. Chim. Acta,* 1993, **203**, 171–174; (b) K. M. Kadish, G. Royal, E. van Caemelbecke and L. Gueletti, in *The Porphyrin Handbook*; K. M. Kadish, K. M. Smith, R. Guilard (eds.); Academic Press: San Diego, CA (USA), 2000, **9**, pp.1 – 219.

[9] Loutfyc, R.O.; Hsiaob, K.; Ong, S.; Keoshkeria, B. *Can. J .Chem.* **1984**, *62***,** 1877– 1885.

[10] (a) A. B. P. Lever, E. R. Milaeva, G. Speier, In Phthalocyanines: Properties and Applications; Leznoff, C. C., Lever, A. B. P., Eds.; VCH Publishing: Weinheim, *1993*; Vol. *3*, pp. 1−70; (b) J. Shen, J. Shao, Z. Ou, W. E, B. Koszarna, D. T. Gryko and K. M. Kadish, Ou, W. E, B. Koszarna, D. T. Gryko and K. M. Kadish, *Inorg. Chem.* **2006**, *45*, 2251–2265.

[11] M. A. Faraonov, D. V. Konarev, S. S. Khasanov, S. I. Troyanov, R. N. Lyubovskaya *Dalton Trans*, 2017, **46**, 3547-3555.

[12] (a) M. -H. Whangbo, R. Hoffmann, *J. Am. Chem. Soc.* **1978**, *100*, 6093-6098; (b) Crystal and Electronic Structure Analysis Using CAESAR, J. Ren, W. Liang, M. -H. Whangbo, **1998**, Prime Color Software, Inc. (this book can be downloaded free of charge from the website: http://www.PrimeC.com/). Default parameters were used.

[13] S. Matsumoto, K. Matsuhama and J. Mizuguchi, *Acta Crystallogr.,Sect. C: Cryst. Struct.Commun.* **1999**, *55*, 131–133.

[14] a) M. Nakano, H. Fukui, T. Minami, K. Yoneda, Y. Shigeta, R. Kishi, B. Champagne, E. Botek, T. Kubo, K. Ohta, K. Kamada, *Theor. Chem. Acc.* **2011**, *130*, 711–724; b) M. Nakano, T. Minami, H. Fukui, K. Yoneda, Y. Shigeta, R. Kishi, B. Champagne, E. Botek, *Chem. Phys. Lett.* **2010**, *501*, 140–145; c) K. Yoneda, M. Nakano, Y. Inoue, T. Inui, K. Fukuda, Y. Shigeta, T. Kubo, B. Champagne, *J. Phys. Chem. C* **2012**, *116*, 17787–17795.

[15] (a) M. Bendikov, H. M. Duong, K. Starkey, K. N. Houk, E. A. Carter, F. Wudl, *J. Am. Chem. Soc*., **2004**, *126*, 7416–7417; (b) A. Shimizu, T. Kubo, M. Uruichi, K. Yakushi, M. Nakano, D. Shiomi, K. Sato, T. Takui, Y. Hirao, K. Matsumoto, H. Kurata, Y. Morita. K. Nakasuji, *J. Am. Chem. Soc*., **2010**, *132*, 14421–14421.

[16]. (a) S. Will, J. Lex, E. Vogel, H. Schmickler, J. P. Gisselbrecht, C. Haubtmann, M. Bernard, M. Gross, *Angew. Chem., Int. Ed. Engl.,* 1997, **36**, 357–361; (b) F. Jérôme, J.-M. Barbe, C. P. Gros, R.; Guilard, J. Fisher, R. Weiss, *New J. Chem.,* 2001, **25**, 93–101; (c) S. Hiroto, K. Furukawa, H. Shinokubo, A. Osuka, *J. Am. Chem. Soc*., 2006, **128**, 12380–12381.

[17] D. V. Konarev, S. S. Khasanov, E. I. Yudanova, R. N. Lyubovskaya, *Eur. J. Inorg. Chem.,* **2011**, 816 – 820.

[18] Bruker AXS Inc., Madison, Wisconsin, USA.

[19] G. M. Sheldrick, *Acta Crystallogr., Sect. A: Fundam. Crystallogr.* **2008**, *64*, 112 – 122.

Entry for the Table of Contents

Macroheterocycles

Salt $(PPN^{+})_2(H_2Nc^{2-})$ (**1**) containing free-base naphthalocyanine H_2Nc^{2-} dianions was obtained. It forms as a result of the disproportionation reaction of $H_2Nc^{\bullet-}$ to H_2Nc^{0} and H_2Nc^{2-}. The H_2Nc^{2-} macrocycle shows essential distortion due to the formation of oppositely located short and long C-N_{imine} bonds. Distortion increases with the negative charge on H_2Nc. Macrocycle has diamagnetic singlet ground state and the lowest energy absorption band at 1230 nm.

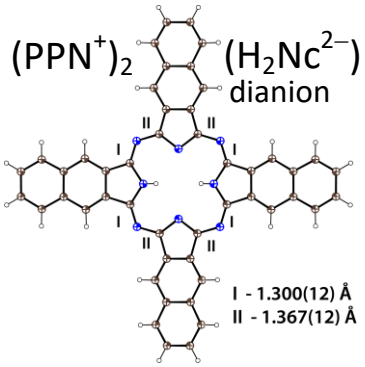

D.V. Konarev, S.S. Khasanov, Y. Nakano, A. F. Shestakov, M. Ishikawa, A. Otsuka, H. Yamochi, H. Kitagawa, R. N. Lyubovskaya[a]

Page No. – Page No.

Molecular structure, optical and magnetic properties of free-base naphthalocyanine H_2Nc^{2-} dianions

IR- spectra.

Table S1. IR-spectra (cm^{-1} in KBr) of starting compounds and salt **1**.

	H_2Nc	PPNCl	$(PPN^+)_2(H_2Nc^{2-})$ (**1**)
Naphthalo-cyanine	471s		471m
	497w		488m
	614w		612w
	695m		691s*
	719w		721s*
	754s		750m
	832m		825w
	890s		880m
	1005s		997m*
	1027s		1027w*
	1092s		1087s
	1144w		1144w
	1164w		1159m
	1213w		1219m
	1263w		1262m*
	1327m		1324w
	1352s		-
	1368m		1373s
	1392s		1384s
	1441w		1436m*
	1469w		1469w
	1497w		1498w*
	1516m		-
	1532s		-
	3052w		3046w*
	3290w		Not well resolved
PPN^+		500s	500m
		531s	533s
		550s	546m
		694m	691s*
		724m	721s*
		746m	742m
		754m	750m*
		-	779s
		-	986m
		997m	997m*
		1024w	1027w*
		1075w	-
		1115s	1116m
		-	1194m
		1262s	1262m*
		-	1429m
		1439s	1436m*
		1483m	1498w*
		1587m	-
		3046w	3046w*

w – weak, m-middle, s – strong intensity.

*- bands are coincided

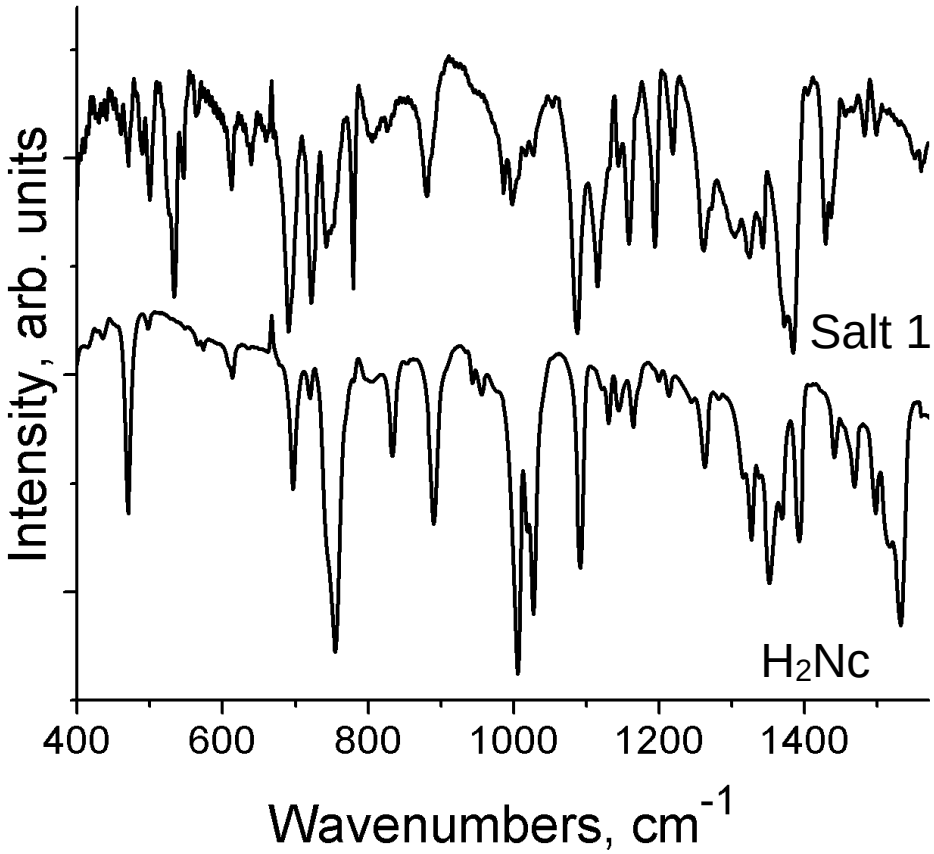

Figure S1. IR-spectrum of pristine H_2Nc and salt $(PPN^+)_2(H_2Nc^{2-})$ (**1**) in KBr pellets. Pellet for **1** was prepared in anaerobic conditions.

.

Crystal structure of 1.

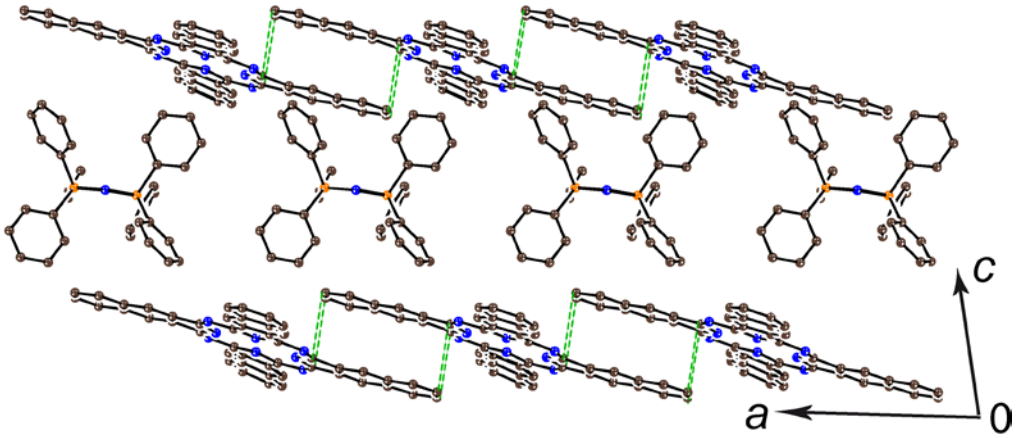

Figure S2. View along the naphthalocyanine and cationic layers in $(PPN^{+})_2(H_2Nc^{2-})$ (**1**).

Theoretical calculations.

For the quantum-chemical simulation, the PBE density functional method[1] was applied using the three-exponential basis with the polarization functions C, N, (5s, 5p, 2d) / [3s, 3p, 2d], H (5s, 1p) / [3s, 1p] for valence electrons and the core SBK-JC pseudopotential[2]. All calculations were performed with the help of the program package PRIRODA[3] using computing facilities of Joint Supercomputer Center of RAS. Atomic distribution of charge was determined by the Hirschfeld method.[4]

Cartesian coordinates (in Å), for all calculated structures (see Figures **S3-S6**) are listed in the Table **S2**.

The calculated frequencies ν, in cm^{-1}, of IR-active vibrations (with intensities I ≥ 10 km/mol) are given in the Table **S3** together with corresponding effective mass μ (in a.u.m.).

About half of an additional electronic density of the $H_2Nc^{\bullet-}$ and H_2Nc^{2-} anions is located on nitrogen (10%) and carbon atoms (21 %) of the pyrrole rings. These values slightly change for the H_2Nc^{2-} dianion in triplet state, which corresponds to the higher localization of LUMO+1 orbital on nitrogen (14%) and same of the carbon atoms (20%). That is the reason why bonding and antibonding properties of LU and LU+1 orbitals are not strictly the same providing elongation of the C-N_{imine} and C-N_{pyr} bonds in the triplet H_2Nc^{2-} dianion by 0.003 - 0.009 Å (0.0075 Å in average). Elongation of the bonds in the singlet H_2Nc^{2-} dianions is the same and by about two times larger than that in the H_2Nc^{-} radical anion for the reason of more antibonding nature of populated LU and LU+1 orbitals are than bonding.

The PBE functional indicates that gap between LU and LU+1 orbitals of H_2Nc is very small, 0.095 eV only. This lead to relatively small vertical S-T splitting in H_2Nc^{2-} of 450 and 1265 K at the geometry of H_2Nc and H_2Nc^{2-}, respectively.

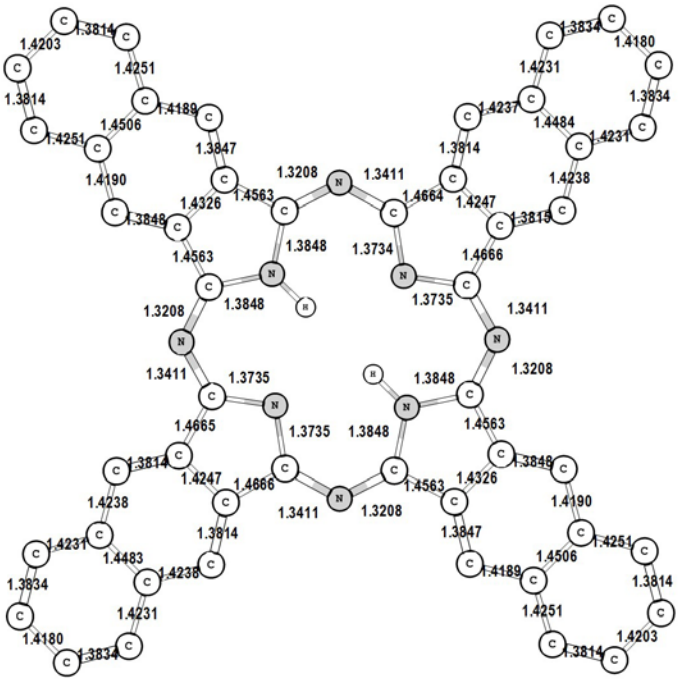

Figure S3. Geometry of pristine neutral H_2Nc according to the DFT calculations.

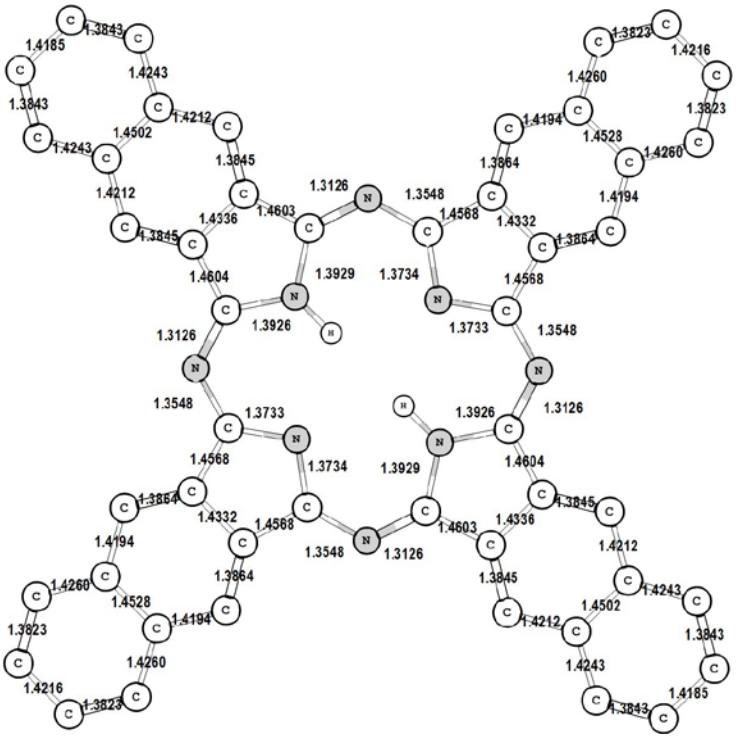

Figure S4. Geometry of the $H_2Nc^{\bullet-}$ radical anion according to the DFT calculations.

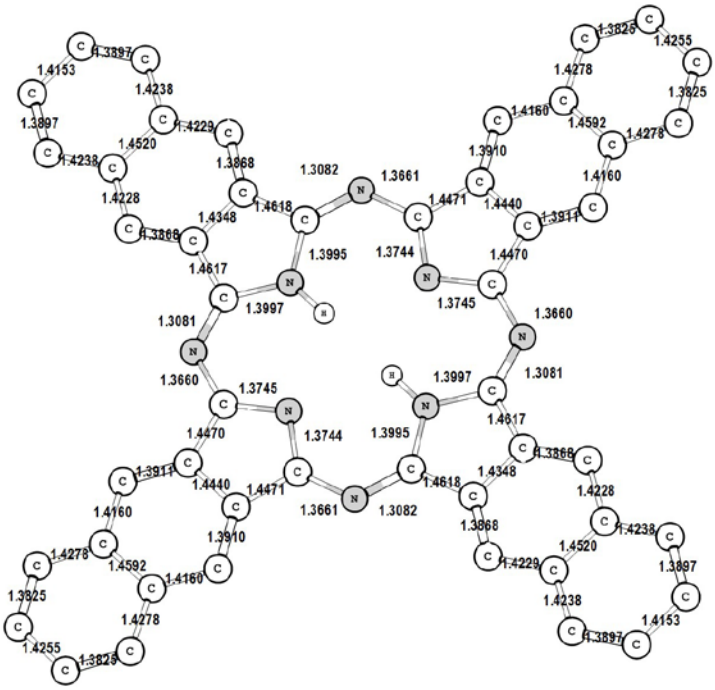

Figure S5. Geometry of the H_2Nc^{2-} dianion in singlet ground state according to the DFT calculations.

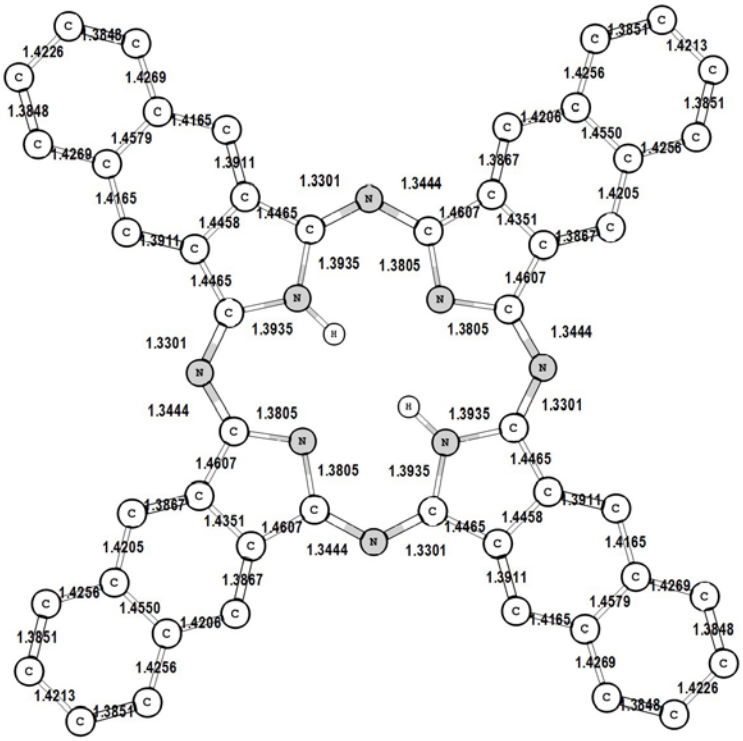

Figure S6. Geometry of the H_2Nc^{2-} dianion in triplet excited state according to the DFT calculations.

Calculated IR spectra.

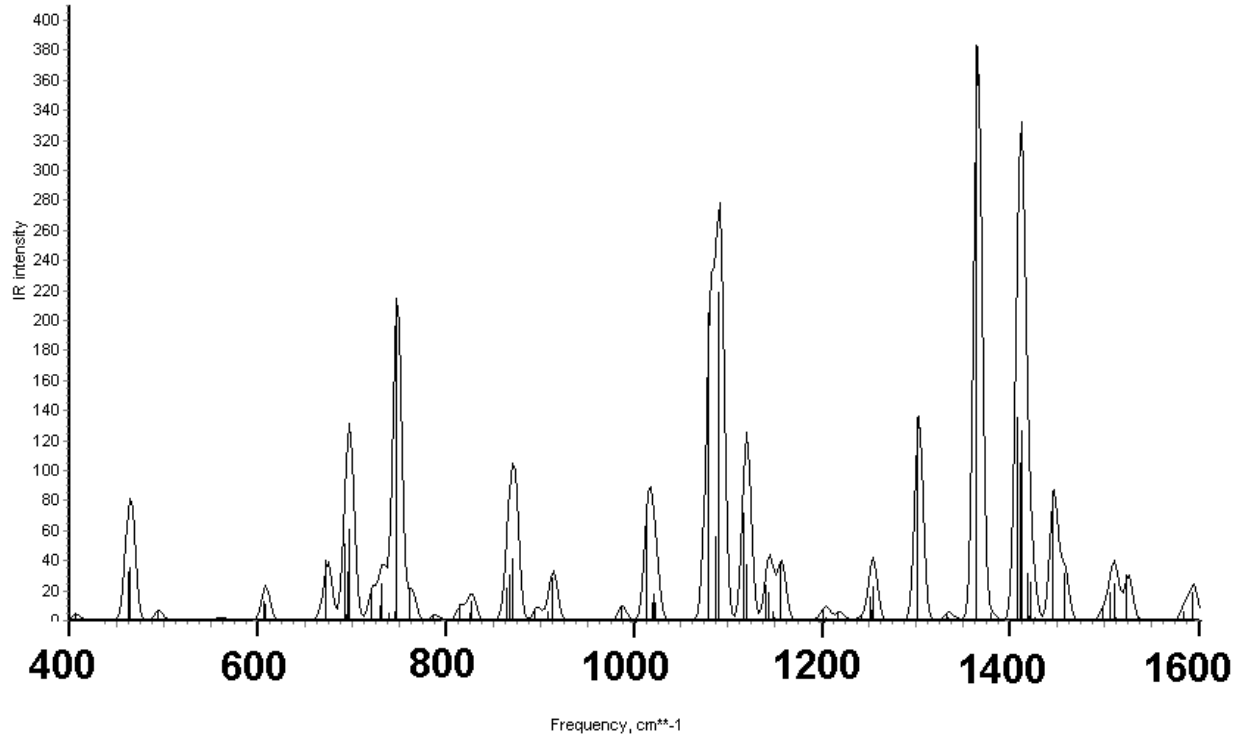

Figure S7. Calculated IR spectrum of pristine neutral H_2Nc according to the DFT calculations.

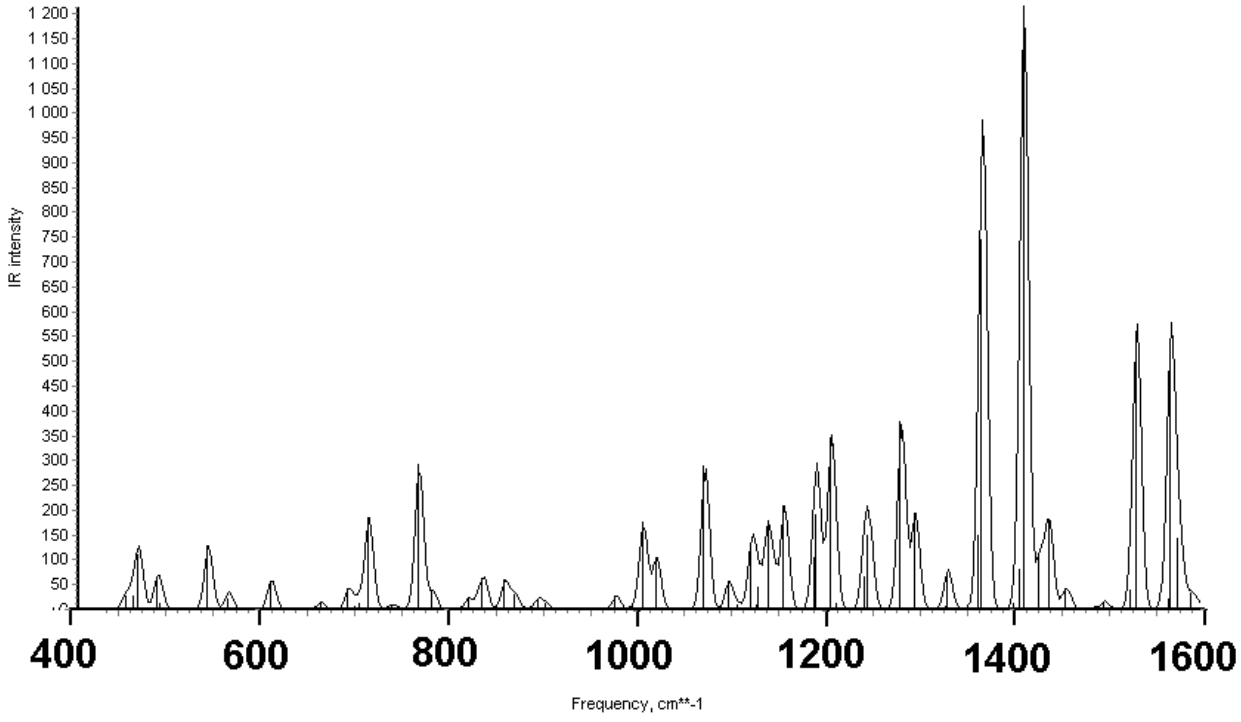

Figure S8. Calculated IR spectrum of the H_2Nc^{2-} dianions according to the DFT calculations.

Calculated IR spectra show rather good correspondence with experimentally observed IR spectra of pristine H_2Nc and the H_2Nc^{2-} dianions in the spectrum of salt **1**. Most intense bands at 471, 754, 890, 1005, 1092, 1352, 1392 cm^{-1} are reproduced in the theoretical spectrum of H_2Pc excepting bands at 1027 and 1532 cm^{-1}. In the spectrum of **1** most intense bands of H_2Nc^{2-} at 721, 1087, 1373 and 1384 cm^{-1} are also reproduced in the theoretical spectrum excepting bands at 691 cm-1 and bans in the 1500-1600 cm^{-1}.

Table S2. Atomic numbers Z and Cartesian coordinates

neutral H_2Nc

Z	Cartesian coordinates in Å		
7	8.36325537	4.26468918	7.69630595
7	8.42840590	2.41386996	9.27545767
7	8.34246402	4.50953959	10.51734665
7	8.27622191	6.01828987	12.43072319
7	8.22948249	7.34065933	10.38721209
7	8.16639722	9.19294003	8.80929278
7	8.25733196	7.09744350	7.56821441
7	8.32862591	5.58846534	5.65551651
6	8.36776595	4.45033357	6.32370016
6	8.42405113	3.11860246	5.73721582
6	8.45428721	2.17473317	6.81474997
6	8.41552421	2.92977241	8.05950403
6	8.39457127	3.14188994	10.40136689
6	8.41166539	2.50903615	11.72434962
6	8.36652466	3.58074023	12.66199451
6	8.32420011	4.80656944	11.85805259
6	8.23396787	7.15498329	11.75953090
6	8.18058802	8.48668326	12.34659120
6	8.14806777	9.43096068	11.26980925
6	8.18126439	8.67624053	10.02486484
6	8.20130086	8.46505866	7.68337404
6	8.18322358	9.09721131	6.36000746
6	8.23115488	8.02491224	5.42324719
6	8.27618694	6.79972021	6.22777324
6	8.44538580	2.70173366	4.41687249
1	8.42582165	3.42675707	3.60140217
6	8.49701620	1.31099611	4.14037184
6	8.52836465	0.35534183	5.23127742
6	8.50557269	0.81201056	6.57454850
1	8.52465547	0.09940174	7.40093485
6	8.46583552	1.19156169	12.13637736
1	8.50175108	0.37472740	11.41301841
6	8.47362131	0.91428410	13.53283718
6	8.42860777	2.00384993	14.48595194
6	8.37533088	3.34948294	14.02383815
1	8.34513681	4.17543296	14.73703885
6	8.15655379	8.90256873	13.66720438
1	8.18420433	8.17715273	14.48211319
6	8.09863430	10.29283847	13.94459191
6	8.06429796	11.24899266	12.85415270
6	8.09050014	10.79338342	11.51062483
1	8.06211781	11.50610104	10.68461779
6	8.14049954	10.41455604	5.94618465
1	8.10397125	11.23263778	6.66810359
6	8.14338861	10.69037520	4.54924984
6	8.19210476	9.59989115	3.59715826
6	8.23739364	8.25471602	4.06117514
1	8.27967762	7.42647919	3.35127532

1	8.26311265	6.57441209	9.71237707
1	8.32994995	5.03163217	8.37039327
6	8.44112281	1.69600235	15.87531350
1	8.40777830	2.51895208	16.59276884
6	8.49536547	0.38594219	16.31630389
6	8.53034274	-0.41998600	14.02469481
1	8.50508293	0.16908620	17.38576574
1	8.56517793	-1.24071957	13.30478351
6	8.53903574	-0.68091619	15.38317246
1	8.58204405	-1.71075168	15.74163899
6	8.58244973	-1.03423030	4.92027200
1	8.60371049	-1.75257470	5.74261961
6	8.60599025	-1.47031738	3.60968580
6	8.52155183	0.82080922	2.80246517
1	8.64676378	-2.53834607	3.38973280
1	8.49353856	1.54112619	1.98210680
6	8.57824630	-0.53460469	2.54161468
1	8.59772600	-0.89250638	1.51095215
6	8.19514236	9.90691533	2.20765596
1	8.23333973	9.08347038	1.49102708
6	8.10163856	12.02464708	4.05616318
6	8.15234431	11.21704216	1.76547617
1	8.06774359	12.84628940	4.77506954
1	8.15647655	11.43329182	0.69584003
6	8.10290080	12.28462389	2.69737891
1	8.06967508	13.31443166	2.33784165
6	8.00437408	12.63824116	13.16595822
1	7.97702062	13.35678945	12.34396816
6	8.06902684	10.78218253	15.28271018
6	7.97913781	13.07355820	14.47671904
1	8.09245105	10.06114192	16.10260715
1	7.93205431	14.14119390	14.69728611
6	8.01439064	12.13747052	15.54433646
1	7.99407878	12.49468041	16.57522862

$H_2Nc^{\bullet-}$ radical anion

Z	**Cartesian coordinates in Å**		
7	8.36505733	4.26604055	7.69713487
7	8.43030193	2.40276789	9.26723559
7	8.34255081	4.50068646	10.52889439
7	8.27484501	6.02874925	12.44246046
7	8.23145448	7.33835712	10.38686531
7	8.16778689	9.20155187	8.81683533
7	8.25685526	7.10372164	7.55515729
7	8.32827117	5.57576774	5.64157851
6	8.36763950	4.45068759	6.31643527
6	8.42345081	3.11305772	5.73351887
6	8.45412118	2.16909962	6.81207513
6	8.41668872	2.92296672	8.06222559
6	8.39578075	3.13398469	10.40737709
6	8.41325127	2.50622723	11.72195520
6	8.36704738	3.58383666	12.66565767

6	8.32416182	4.80256993	11.86869816
6	8.23382691	7.15374737	11.76758732
6	8.17943196	8.49142006	12.35057555
6	8.14770432	9.43541874	11.27207658
6	8.18219316	8.68151596	10.02188344
6	8.20224328	8.47037103	7.67669993
6	8.18479809	9.09814724	6.36211249
6	8.23229277	8.02056115	5.41843634
6	8.27606140	6.80183474	6.21533162
6	8.44450206	2.69262675	4.41448558
1	8.42228476	3.41924559	3.59997624
6	8.49790044	1.30037815	4.13420307
6	8.52910462	0.34558303	5.22524297
6	8.50595503	0.80705588	6.56926159
1	8.52651882	0.09607273	7.39749891
6	8.46738391	1.18628626	12.14248667
1	8.50371314	0.36939228	11.41837527
6	8.47483313	0.90818104	13.53437180
6	8.42861866	2.00053423	14.49107979
6	8.37499124	3.34216600	14.03084127
1	8.34267687	4.16754021	14.74546188
6	8.15438601	8.91160899	13.66961184
1	8.17993518	8.18505581	14.48408237
6	8.09719725	10.30368882	13.94998554
6	8.06409482	11.25848812	12.85901100
6	8.09077773	10.79724768	11.51498048
1	8.06428642	11.50806942	10.68677370
6	8.14169838	10.41847859	5.94148894
1	8.10634114	11.23554295	6.66544812
6	8.14326120	10.69677643	4.54961872
6	8.19162378	9.60447153	3.59299308
6	8.23667312	8.26254222	4.05328912
1	8.27656311	7.43733415	3.33886552
1	8.26663119	6.57230310	9.71450791
1	8.33344095	5.03238440	8.36933365
6	8.44033495	1.68558747	15.88184721
1	8.40606156	2.50911087	16.59984074
6	8.49429601	0.37710740	16.32413582
6	8.53075699	-0.42727821	14.03123918
1	8.50267192	0.16061413	17.39445514
1	8.56563303	-1.24750470	13.30951308
6	8.53938052	-0.69181269	15.38793835
1	8.58273224	-1.72301161	15.74467932
6	8.58303262	-1.04291478	4.91265911
1	8.60491532	-1.76027256	5.73669139
6	8.60627158	-1.48427835	3.60076411
6	8.52318937	0.80740870	2.79815987
1	8.64751116	-2.55365938	3.38420007
1	8.49817129	1.52890376	1.97783939
6	8.57741429	-0.55031814	2.53357976
1	8.59508197	-0.90601324	1.50141868
6	8.19364481	9.91988664	2.20227171

1	8.23121093	9.09640540	1.48439579
6	8.10032838	12.03273064	4.05273315
6	8.15062137	11.22875593	1.75995833
1	8.06485844	12.85297853	4.77440798
1	8.15350410	11.44562063	0.68968628
6	8.10232164	12.29761094	2.69608297
1	8.06965496	13.32920752	2.33935310
6	8.00509383	12.64676252	13.17167345
1	7.97917244	13.36402272	12.34767285
6	8.06821984	10.79640350	15.28604747
6	7.97925089	13.08792082	14.48358788
1	8.09266749	10.07482157	16.10630830
1	7.93346106	14.15710470	14.70021155
6	8.01237942	12.15404598	15.55072436
1	7.99070362	12.50950611	16.58288985

H_2Nc^{2-} dianion in singlet state

Z	**Cartesian coordinates in Å**		
7	8.36497732	4.26761644	7.69785828
7	8.43103108	2.39233378	9.25998040
7	8.34287538	4.49193827	10.53997337
7	8.27426828	6.03738686	12.45329397
7	8.23151338	7.33650567	10.38624937
7	8.16765864	9.21187300	8.82412395
7	8.25659809	7.11230195	7.54417757
7	8.32848186	5.56701076	5.63086410
6	8.36749204	4.44966291	6.31001440
6	8.42324371	3.10943541	5.72944966
6	8.45398356	2.16490027	6.80911107
6	8.41689690	2.91727624	8.06191123
6	8.39638375	3.12461103	10.41276549
6	8.41389348	2.50175851	11.71886087
6	8.36721427	3.58728412	12.66999273
6	8.32430205	4.79868748	11.87973262
6	8.23353218	7.15464392	11.77408642
6	8.17885796	8.49498338	12.35461070
6	8.14721456	9.43948253	11.27493286
6	8.18197454	8.68694098	10.02218945
6	8.20219119	8.47959312	7.67134591
6	8.18506645	9.10244023	6.36525737
6	8.23281154	8.01695757	5.41414173
6	8.27602017	6.80556896	6.20442799
6	8.44456529	2.68362440	4.40976803
1	8.42199599	3.41118553	3.59548836
6	8.49827919	1.29064460	4.12493819
6	8.52950554	0.33484809	5.21753214
6	8.50606894	0.80141929	6.56153590
1	8.52685204	0.09109268	7.39094220
6	8.46801815	1.17999753	12.14893617
1	8.50443798	0.36202527	11.42488232
6	8.47545897	0.90101128	13.53717331
6	8.42887821	1.99795386	14.49830849

6	8.37532870	3.33600777	14.03815168
1	8.34266795	4.16130932	14.75402387
6	8.15353899	8.92066672	13.67425805
1	8.17886046	8.19322724	14.48856573
6	8.09640045	10.31352259	13.95904124
6	8.06348210	11.26923901	12.86642500
6	8.09036591	10.80278354	11.52244559
1	8.06421370	11.51288393	10.69299674
6	8.14184621	10.42461781	5.93525154
1	8.10657841	11.24264442	6.65930466
6	8.14318381	10.70395424	4.54706315
6	8.19170040	9.60708818	3.58593866
6	8.23660311	8.26870276	4.04604670
1	8.27611612	7.44365780	3.33022462
1	8.26695457	6.57169652	9.71563717
1	8.33375584	5.03264423	8.36842767
6	8.44065659	1.67682592	15.88946655
1	8.40619028	2.50147591	16.60770058
6	8.49452804	0.36913555	16.33486786
6	8.53122956	-0.43422921	14.03966461
1	8.50265173	0.15371101	17.40636254
1	8.56618989	-1.25460501	13.31657198
6	8.53992115	-0.70250999	15.39588574
1	8.58335139	-1.73516316	15.75127876
6	8.58344747	-1.05253555	4.90242390
1	8.60555245	-1.76964672	5.72764737
6	8.60673983	-1.49919814	3.58663456
6	8.52363412	0.79483761	2.79049883
1	8.64812175	-2.57018899	3.37311341
1	8.49887329	1.51725833	1.96999724
6	8.57769866	-0.56754331	2.52167912
1	8.59500266	-0.92082220	1.48764210
6	8.19339195	9.92876694	2.19485928
1	8.23088077	9.10428296	1.47658784
6	8.10016636	12.03971573	4.04467399
6	8.15040158	11.23689206	1.74955773
1	8.06451863	12.86000301	4.76782949
1	8.15318174	11.45275615	0.67812495
6	8.10213249	12.30843225	2.68851600
1	8.06947539	13.34150129	2.33316921
6	8.00475757	12.65643856	13.18148849
1	7.97915972	13.37340104	12.35623676
6	8.06739037	10.80920399	15.29345290
6	7.97861846	13.10300575	14.49725721
1	8.09188406	10.08678443	16.11396302
1	7.93306529	14.17383429	14.71074303
6	8.01128767	12.17150799	15.56224389
1	7.98951688	12.52462559	16.59625168

-

H_2Nc^{2-} dianion in triplet state

Z	**Cartesian coordinates in Å**		

7	8.36618050	4.25640761	7.68781681
7	8.43162008	2.39206413	9.27923027
7	8.34296484	4.50235331	10.52740431
7	8.27460681	6.01758740	12.45579840
7	8.23161766	7.34752586	10.39642838
7	8.16848844	9.21176541	8.80484819
7	8.25740581	7.10152389	7.55680354
7	8.32741049	5.58653308	5.62831572
6	8.36780884	4.44340351	6.30701506
6	8.42301984	3.11814301	5.72956798
6	8.45413983	2.16638487	6.81734551
6	8.41762801	2.91337366	8.05564514
6	8.39694202	3.12830969	10.40361826
6	8.41455359	2.50310380	11.72340644
6	8.36780032	3.58214986	12.66857143
6	8.32418857	4.80671173	11.87381631
6	8.23319869	7.16093919	11.77737006
6	8.17910859	8.48624485	12.35460326
6	8.14751708	9.43781978	11.26666944
6	8.18229768	8.69059227	10.02843095
6	8.20302187	8.47548969	7.68056357
6	8.18595884	9.10090739	6.36087695
6	8.23317787	8.02196383	5.41564466
6	8.27656300	6.79741563	6.21025778
6	8.44512440	2.68582900	4.40757039
1	8.42179084	3.41142901	3.59117847
6	8.49950417	1.29841040	4.12714563
6	8.53087759	0.33864179	5.22407657
6	8.50711473	0.79974485	6.56325493
1	8.52884134	0.08692175	7.39087552
6	8.46792305	1.18382652	12.14743050
1	8.50434948	0.36819958	11.42099206
6	8.47480021	0.90183886	13.53967410
6	8.42774775	1.99581046	14.49776868
6	8.37450493	3.33723578	14.03346089
1	8.34067282	4.16498216	14.74617915
6	8.15378653	8.91871952	13.67651336
1	8.17824958	8.19333248	14.49305968
6	8.09748794	10.30609941	13.95671386
6	8.06502327	11.26562796	12.85961844
6	8.09126299	10.80435785	11.52053843
1	8.06596522	11.51689256	10.69277076
6	8.14188483	10.42055988	5.93698618
1	8.10697377	11.23618316	6.66349628
6	8.14220837	10.70297511	4.54480393
6	8.19026056	9.60913264	3.58663648
6	8.23591199	8.26738832	4.05082039
1	8.27434891	7.43990247	3.33803842
1	8.26721635	6.58006633	9.72416282
1	8.33492817	5.02383228	8.36032092
6	8.43800519	1.67825874	15.88747675
1	8.40291622	2.50321576	16.60493145

6	8.49121309	0.36814696	16.33406021
6	8.52943898	-0.43221219	14.03924065
1	8.49811266	0.15362832	17.40569067
1	8.56473877	-1.25229281	13.31621698
6	8.53712286	-0.70052636	15.39813405
1	8.57985040	-1.73327695	15.75318044
6	8.58534144	-1.05099914	4.90447790
1	8.60796301	-1.76875600	5.72958054
6	8.60865666	-1.49586555	3.59327390
6	8.52533736	0.79829840	2.79095078
1	8.65044138	-2.56654476	3.37818261
1	8.50123322	1.52077620	1.97001560
6	8.57897533	-0.55925130	2.52287465
1	8.59654960	-0.91376025	1.48925002
6	8.19082289	9.92720993	2.19700650
1	8.22770964	9.10237760	1.47949737
6	8.09823306	12.03747472	4.04540548
6	8.14704154	11.23772032	1.75058082
1	8.06246515	12.85747137	4.76850048
1	8.14875846	11.45265833	0.67901394
6	8.09955328	12.30626158	2.68658230
1	8.06614973	13.33940356	2.33167506
6	8.00710119	12.65518504	13.17894052
1	7.98224226	13.37269982	12.35369184
6	8.06898346	10.80634505	15.29281110
6	7.98136916	13.10019912	14.49005202
1	8.09337221	10.08402756	16.11387952
1	7.93670110	14.17080309	14.70493426
6	8.01342462	12.16386385	15.56063215
1	7.99195426	12.51840247	16.59417348

Table S3. Calculated frequencies ν, in cm-^{1}, effective masses μ, in a.u.m and intensities I, in km/mol of most intense IR vibrations

H_2Nc			H_2Nc^{2-}		
ν, cm-1	μ, a.u.m	I, km/mol	ν, cm-1	μ, a.u.m	I, km/mol
464	2.65	32	452	2.63	27
464	7.97	14	460	2.68	28
465	2.66	35	465	8.20	111
609	6.78	13	486	6.59	63
609	6.75	11	489	7.24	12
674	2.39	40	539	1.23	128
694	1.62	51	561	6.53	14
698	7.32	33	562	6.53	22
699	8.23	60	608	6.77	10
722	1.45	22	608	6.79	51
732	2.15	10	661	3.05	14
733	1.55	25	690	1.88	42
748	3.34	215	702	1.42	11
764	4.84	22	712	2.67	184
816	4.78	10	737	6.13	10
828	4.77	13	765	4.66	293
866	1.50	22	780	5.60	38
870	1.48	30	819	4.65	21
872	1.47	32	834	1.43	64
873	1.57	42	858	1.49	59
914	1.42	29	869	1.40	30
1015	5.12	71	893	4.17	21
1021	2.30	12	902	5.48	13
1023	2.23	18	977	3.23	27
1024	2.22	11	1006	2.26	175
1081	2.20	205	1021	2.19	105
1089	2.31	56	1072	2.24	289
1091	2.86	219	1098	1.93	55
1119	2.17	71	1108	1.59	10
1119	1.85	24	1123	1.71	131
1122	1.77	37	1129	1.08	44
1127	1.57	0	1141	3.62	177
1142	1.45	23	1156	2.00	209
1145	1.10	19	1191	1.51	105
1157	1.97	38	1192	1.62	191
1253	2.06	15	1208	2.31	347
1256	2.08	22	1213	2.96	11
1302	10.04	136	1244	2.05	64
1366	5.59	383	1247	3.06	150
1409	3.68	136	1282	6.92	377
1412	5.24	105	1297	7.95	194
1413	5.09	126	1333	2.50	75
1419	3.03	31	1366	3.47	149

1423	2.78	25	1369	5.15	135
1447	4.87	86	1369	6.96	745
1458	4.09	31	1403	5.80	12
1507	4.52	19	1411	2.99	79
1512	4.38	24	1414	4.69	1166
1525	6.87	31	1431	5.78	108
1595	8.82	19	1441	5.02	180
			1459	4.89	42
			1500	4.06	16
			1529	7.34	38
			1535	10.30	560
			1569	8.24	22
			1571	8.70	538
			1580	7.53	143
			1593	6.37	33
			1601	6.64	10
			1636	8.44	617

Computational

DFT and TD-DFT calculations based on the CAM-B3LYP[5] and M11[6] functional were performed using the cc-pVDZ[7] basis set. Partial geometry optimizations on the coordinates of hydrogen atoms in C_2-symmetric H_2Nc^{2-} based on the X-ray structures and full geometry optimizations in H_2Nc^{2-} and oligoacenes were performed with “Opt = Tight” keyword. In the present calculations, “Int =SuperFineGrid” was specified, and stabilities of the wave functions were confirmed by specifying the “Stable = Opt” keyword. Sixty excited states were calculated in the TD-DFT calculation. The subsequent natural bond orbital (NBO) analysis was performed using the NBO program.[8] The computations were performed with the Gaussian 09 program package.[9]

Table S4. Method, point group, state, number of imaginary frequency (NImag), total and relative energy (E and ΔE), and $\langle S^2 \rangle$ value of H_2Nc^{2-} and oligoacenes calculated at the CAM-B3LYP and M11/cc-pVDZ levels of theory.

Method	Point group	State	NImag	E / hartree	ΔE / K	$\langle S^2 \rangle$
H_2Nc^{2-}						
UCAM-B3LYP	C_2	^{3}B	–[b]	−2281.80549	5242	2.010
RCAM-B3LYP	C_2	^{1}A	–[b]	−2281.82209	0	0
UCAM-B3LYP	C_2	BS-singlet[a]	–[b]	−2281.82363	−487	0.645
UM11	C_2	^{3}B	–[b]	−2281.70602	6796	2.017
RM11	C_2	^{1}A	–[b]	−2281.72754	0	0
UM11	C_2	BS-singlet[a]	–[b]	−2281.72874	−380	0.590
UCAM-B3LYP	D_{2h}	$^3B_{3g}$	1	−2281.83008	3716	2.005
UCAM-B3LYP	C_{2v}	$^3B_2$	0	−2281.83019	3681	2.023
RCAM-B3LYP	D_{2h}	^1A_g	0	−2281.84185	0	0
UCAM-B3LYP	D_{2h}	BS-singlet[a]	0	−2281.84196	−36	0.486
UM11	D_{2h}	$^3B_{3g}$	2	−2281.73121	5845	2.006
UM11	C_{2v}	$^3B_2$	0	−2281.73211	5560	2.052
RM11	D_{2h}	^1A_g	0	−2281.74971	0	0
UM11	D_{2h}	BS-singlet[a]		–[c]		
Pentacene						
UCAM-B3LYP	D_{2h}	$^3B_{1u}$	0	−846.31508	9023	2.061
RCAM-B3LYP	D_{2h}	^1A_g	0	−846.34365	0	0
UCAM-B3LYP	D_{2h}	BS-singlet[a]	0	−846.34395	−94	0.291
UM11	D_{2h}	$^3B_{1u}$	0	−846.25909	9931	2.067
RM11	D_{2h}	^1A_g	0	−846.29054	0	0
UM11	D_{2h}	BS-singlet[a]	0	−846.29057	−8	0.106
Hexacene						
UCAM-B3LYP	D_{2h}	$^3B_{1u}$	0	−999.87820	5239	2.072
RCAM-B3LYP	D_{2h}	^1A_g	0	−999.89479	0	0
UCAM-B3LYP	D_{2h}	BS-singlet[a]	0	−999.89891	−1302	0.893
UM11	D_{2h}	$^3B_{1u}$	0	−999.81299	6026	2.081
RM11	D_{2h}	^1A_g	0	−999.83208	0	0
UM11	D_{2h}	BS-singlet[a]	0	−999.83561	−1115	0.879
Heptacene						
UCAM-B3LYP	D_{2h}	$^3B_{1u}$	0	−1153.43777	2425	2.082
RCAM-B3LYP	D_{2h}	^1A_g	0	−1153.44545	0	0
UCAM-B3LYP	D_{2h}	BS-singlet[a]	0	−1153.45533	−3121	1.227
UM11	D_{2h}	$^3B_{1u}$	0	−1153.36324	3094	2.090
RM11	D_{2h}	^1A_g	0	−1153.37303	0	0
UM11	D_{2h}	BS-singlet[a]	0	−1153.38257	−3012	1.235
Octacene						
UCAM-B3LYP	D_{2h}	$^3B_{1u}$	0	−1306.99488	294	2.091
RCAM-B3LYP	D_{2h}	^1A_g	0	−1306.99581	0	0
UCAM-B3LYP	D_{2h}	BS-singlet[a]	0	−1307.01196	−5100	1.478
UM11	D_{2h}	$^3B_{1u}$	0	−1306.91091	862	2.101
RM11	D_{2h}	^1A_g	0	−1306.91363	0	0
UM11	D_{2h}	BS-singlet[a]	0	−1306.92977	−5097	1.495

[a] Open-shell broken-symmetry singlet. [b] Only coordinates of hydrogen atoms were optimized from X-ray structure. [c] It was not found.

Table S5. Occupation numbers of natural orbitals, n(HO−1), n(HO), n(LU), and n(LU+1), non-spin-projected and spin-projected diradical characters, y_i and y_i^{SP} (i = 0 and 1)[a,b], for the open-shell broken-symmetry singlet states of H_2Nc^{2-} and oligoacenes calculated at the CAM-B3LYP and M11/cc-pVDZ levels of theory.

	H_2Nc^{2-}[c]	H_2Nc^{2-}[d]	Pentacene	Hexacene	Heptacene	Octacene
CAM-B3LYP						
n(LU+1)	0.035	0.025	0.014	0.055	0.097	0.147
n(LU)	0.291	0.209	0.118	0.407	0.589	0.708
n(HO)	1.709	1.791	1.882	1.593	1.411	1.292
n(HO−1)	1.965	1.975	1.986	1.945	1.903	1.853
y_0	0.291	0.209	0.118	0.407	0.589	0.708
y_1	0.035	0.025	0.014	0.055	0.097	0.147
y_0^{SP}	0.056	0.027	0.008	0.123	0.296	0.462
y_1^{SP}	0.001	0.000	0.000	0.002	0.005	0.012
M11						
n(LU+1)	0.036	0.000	0.005	0.057	0.102	0.154
n(LU)	0.254	0.000	0.041	0.391	0.577	0.692
n(HO)	1.746	2.000	1.959	1.609	1.423	1.308
n(HO−1)	1.964	2.000	1.995	1.943	1.898	1.846
y_0	0.254	0.000	0.041	0.391	0.577	0.692
y_1	0.036	0.000	0.005	0.057	0.102	0.154
y_0^{SP}	0.041	0.000	0.001	0.112	0.283	0.437
y_1^{SP}	0.001	0.000	0.000	0.002	0.006	0.014

[a] $y_i = n(\mathrm{LU}+i) = 2 - n(\mathrm{HO}-i)$. [b] $y_i^{SP} = n^{SP}(\mathrm{LU}+i) = 2 - n^{SP}(\mathrm{HO}-i) = [n(\mathrm{LU}+i)]^2/(1 + S_i^2) = 2 - [n(\mathrm{HO}-i)]^2/(1 + S_i^2)$, $S_i = [n(\mathrm{HO}-i) - n(\mathrm{LU}+i)]/2$. [c] Only coordinates of hydrogen atoms were optimized from X-ray structure.
[d] Full optimization was done.

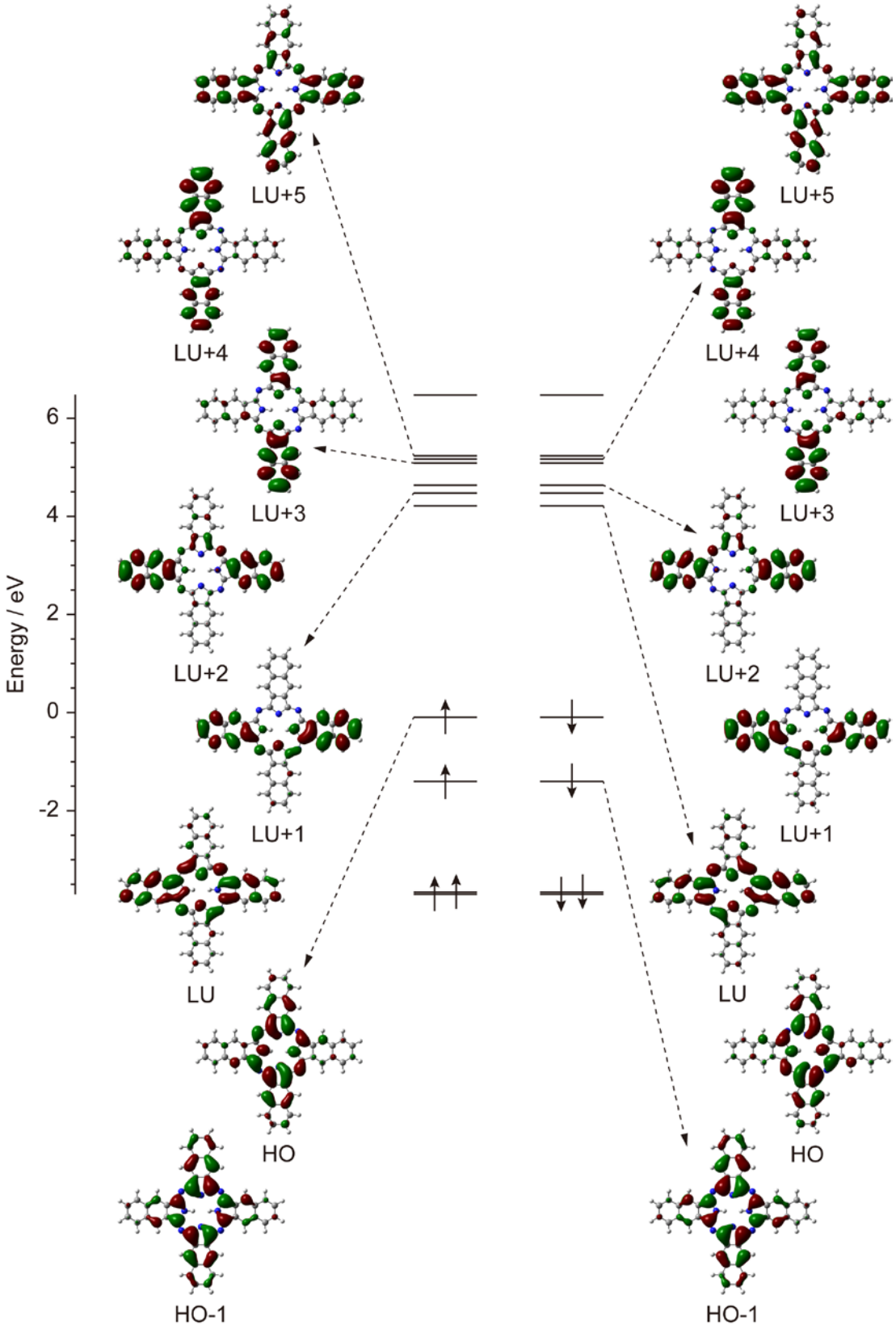

Fig. S9. Energy diagram for the frontier Kohn-Sham orbitals of the broken symmetry singlet state in C_2-symmetric H_2Nc^{2-} calculated at the UCAM-B3LYP/cc-pVDZ level of theory. HO and LU denote the highest occupied and the lowest unoccupied orbitals, respectively.

Table S6. Excitation energies (ΔE), oscillator strengths (f), $\langle S^2 \rangle$ values and assignments on the low-lying excited states for the broken symmetry singlet state of H_2Nc^{2-} calculated at the TD-UCAM-B3LYP/cc-pVDZ level of theory.

	ΔE / eV	ΔE / nm	f	$\langle S^2 \rangle$	Assignment
1	0.627	1979	0.000	1.061	186α → 187α: 41% (α-HO → α-LU) 186β → 187β: 41% (β-HO →β-LU) 186α → 188α: 5% (α-HO → α-LU+1) 186β → 188β: 5% (β-HO → β-LU+1)
2	0.629	1970	0.000	0.412	186α → 187α: 40% (α-HO → α-LU) 186β → 187β: 40% (β-HO →β-LU) 186α → 188α: 4% (α-HO → α-LU+1) 186β → 188β: 4% (β-HO → β-LU+1) 186α → 189α: 3% (α-HO → α-LU+2) 186β → 189β: 3% (β-HO → β-LU+2)
3	1.179	1051	0.011	1.755	186α → 188α: 26% (α-HO → α-LU+1) 186β → 188β: 26% (β-HO → β-LU+1) 186α → 190α: 7% (α-HO → α-LU+3) 186β → 190β: 7% (β-HO → β-LU+3) 185α → 187α: 6% (α-HO−1 → α-LU) 185β → 187β: 6% (β-HO−1 → β-LU) 186α → 187α: 3% (α-HO → α-LU) 186β → 187β: 3% (β-HO →β-LU)
4	1.485	835	0.013	1.988	186α → 190α: 22% (α-HO → α-LU+3) 186β → 190β: 22% (β-HO → β-LU+3) 186α → 188α: 11% (α-HO → α-LU+1) 186β → 188β: 11% (β-HO → β-LU+1) 185α → 191α: 6% (α-HO−1 → α-LU+4) 185β → 191β: 6% (β-HO−1 → β-LU+4)
5	1.495	829	0.000	1.704	186α → 189α: 40% (α-HO → α-LU+2) 186β → 189β: 40% (β-HO → β-LU+2) 186α → 187α: 4% (α-HO → α-LU) 186β → 187β: 4% (β-HO →β-LU)
6	1.544	803	0.004	2.072	186α → 191α: 31% (α-HO → α-LU+4) 186β → 191β: 31% (β-HO → β-LU+4) 185α → 190α: 10% (α-HO−1 → α-LU+3) 185β → 190β: 10% (β-HO−1 → β-LU+3)
7	1.635	758	0.291	0.567	186α → 188α: 39% (α-HO → α-LU+1) 186β → 188β: 39% (β-HO → β-LU+1) 186α → 187α: 3% (α-HO → α-LU) 186β → 187β: 3% (β-HO →β-LU)
8	1.741	712	0.133	1.495	186α → 192α: 17% (α-HO → α-LU+5) 186β → 192α: 17% (α-HO → α-LU+5) 186α → 190α: 17% (α-HO → α-LU+3) 186β → 190β: 17% (β-HO → β-LU+3) 185α → 189α: 4% (α-HO−1 → α-LU+2) 185β → 189β: 4% (β-HO−1 → β-LU+2)
9	1.795	691	0.053	0.869	186α → 189α: 36% (α-HO → α-LU+2) 186β → 189β: 36% (β-HO → β-LU+2) 185α → 187α: 6% (α-HO−1 → α-LU) 185β → 187β: 6% (β-HO−1 → β-LU) 185α → 188α: 3% (α-HO−1 → α-LU+1) 185β → 188β: 3% (β-HO−1 → β-LU+1)
10	1.908	650	0.103	0.860	186α → 190α: 21% (α-HO → α-LU+3) 186β → 190β: 21% (β-HO → β-LU+3) 186α → 192α: 17% (α-HO → α-LU+5)

186β → 192β: 17% (β-HO → β-LU+5)
185α → 187α: 3% (α-HO−1 → α-LU)
185β → 187β: 3% (β-HO−1 → β-LU)
185α → 191α: 3% (α-HO−1 → α-LU+4)
185β → 191β: 3% (β-HO−1 → β-LU+4)

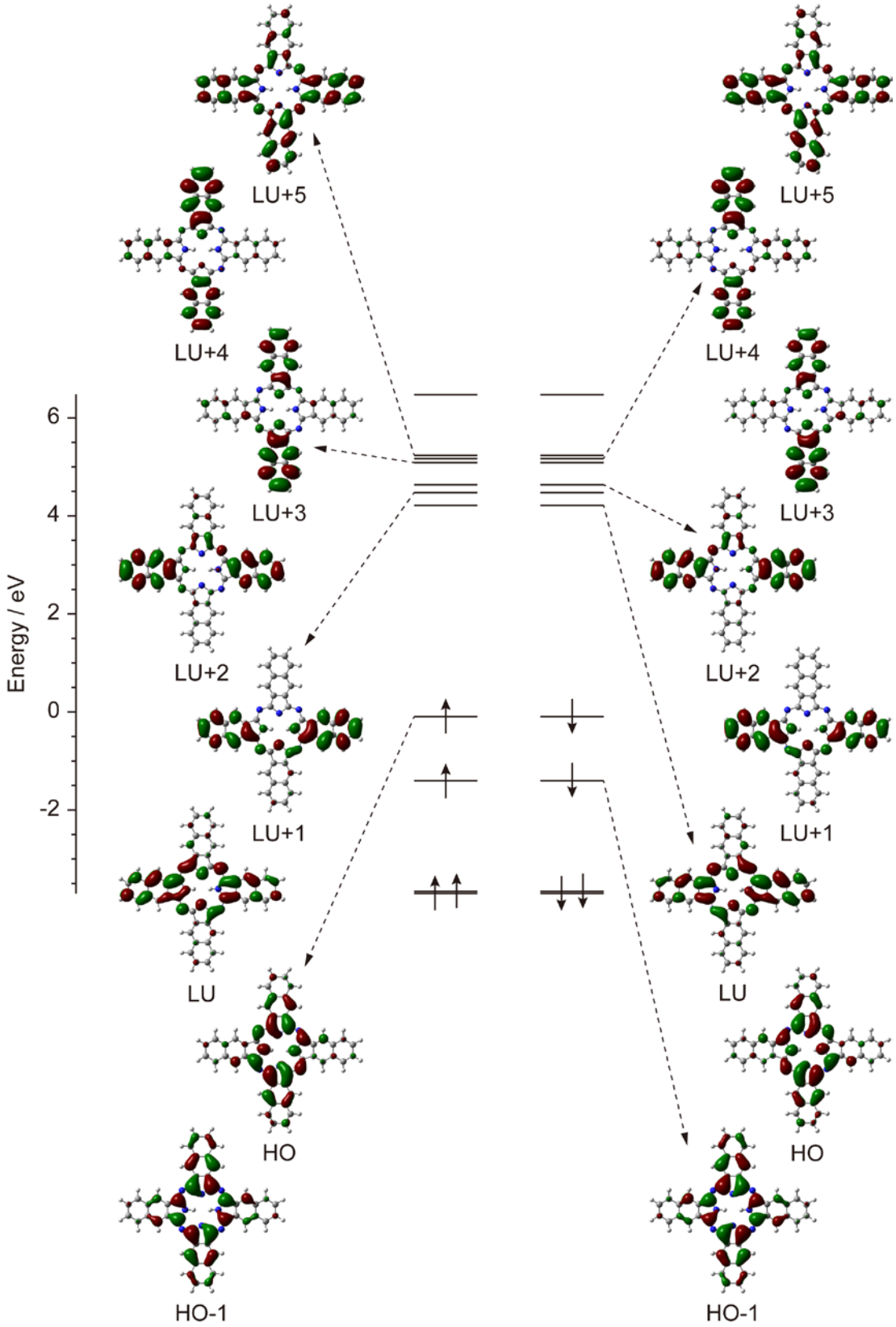

Fig. S10. Energy diagram for the frontier Kohn-Sham orbitals of the broken symmetry singlet state in C_2-symmetric H_2Nc^{2-} calculated at the UM11/cc-pVDZ level of theory. HO and LU denote the highest occupied and the lowest unoccupied orbitals, respectively.

Table S7. Excitation energies (ΔE), oscillator strengths (f), $\langle S^2 \rangle$ values and assignments on the low-lying excited states for the broken symmetry singlet state of H_2Nc^{2-} calculated at the TD-UM11/cc-pVDZ level of theory.

	ΔE / eV	ΔE / nm	f	$\langle S^2 \rangle$	Assignment
1	0.635	1953	0.001	1.143	186α → 187α: 39% (α-HO → α-LU) 186β → 187β: 39% (β-HO →β-LU) 186α → 188α: 4% (α-HO → α-LU+1) 186β → 188β: 4% (β-HO → β-LU+1)
2	0.706	1756	0.000	0.436	186α → 187α: 40% (α-HO → α-LU) 186β → 187β: 40% (β-HO → β-LU) 186α → 188α: 3% (α-HO → α-LU+1) 186β → 188β: 3% (β-HO → β-LU+1)
3	1.339	926	0.031	1.791	186α → 188α: 14% (α-HO → α-LU+1) 186β → 188β: 14% (β-HO → β-LU+1) 185α → 187α: 11% (α-HO−1 → α-LU) 185β → 187β: 11% (β-HO−1 → β-LU) 186α → 190α: 9% (α-HO → α-LU+3) 186β → 190β: 9% (β-HO → β-LU+3) 185α → 191α: 3% (α-HO−1 → α-LU+4) 185β → 191β: 3% (β-HO−1 → β-LU+4) 186α → 192α: 3% (α-HO → α-LU+5) 186β → 192β: 3% (β-HO → β-LU+5)
4	1.722	720	0.001	2.133	186α → 191α: 25% (α-HO → α-LU+4) 186β → 191β: 25% (β-HO → β-LU+4) 185α → 190α: 11% (α-HO−1 → α-LU+3) 185β → 190β: 11% (β-HO−1 → β-LU+3)
5	1.778	697	0.091	1.990	186α → 190α: 17% (α-HO → α-LU+3) 186β → 190β: 17% (β-HO → β-LU+3) 186α → 188α: 14% (α-HO → α-LU+1) 186β → 188β: 14% (β-HO → β-LU+1) 185α → 191α: 7% (α-HO−1 → α-LU+4) 185β → 191β: 7% (β-HO−1 → β-LU+4)
6	1.818	682	0.207	1.812	186α → 189α: 14% (α-HO → α-LU+2) 186β → 189β: 14% (β-HO → β-LU+2) 186α → 192α: 12% (α-HO → α-LU+5) 186β → 192β: 12% (β-HO → β-LU+5) 186α → 190α: 5% (α-HO → α-LU+3) 186β → 190β: 5% (β-HO → β-LU+3) 185α → 189α: 4% (α-HO−1 → α-LU+2) 185β → 189β: 4% (β-HO−1 → β-LU+2)
7	1.908	650	0.164	1.613	186α → 189α: 21% (α-HO → α-LU+2) 186β → 189β: 21% (β-HO → β-LU+2) 186α → 192α: 5% (α-HO → α-LU+5) 186β → 192β: 5% (β-HO → β-LU+5) 186α → 187α: 4% (α-HO → α-LU) 186β → 187β: 4% (β-HO → β-LU) 186α → 190α: 3% (α-HO → α-LU+3) 186β → 190β: 3% (β-HO → β-LU+3)
8	2.013	616	0.307	0.526	186α → 188α: 27% (α-HO → α-LU+1) 186β → 188β: 27% (β-HO → β-LU+1) 186α → 190α: 12% (α-HO → α-LU+3) 186β → 190β: 12% (β-HO → β-LU+3)
9	2.136	580	0.166	1.200	186α → 189α: 24% (α-HO → α-LU+2) 186β → 189β: 24% (β-HO → β-LU+2) 185α → 187α: 11% (α-HO−1 → α-LU)

					185β → 187β: 11% (β-HO−1 → β-LU)
10	2.210	561	0.026	0.587	186α → 190α: 15% (α-HO → α-LU+3) 186β → 190β: 15% (β-HO → β-LU+3) 186α → 192α: 10% (α-HO → α-LU+5) 186β → 192β: 10% (β-HO → β-LU+5) 186α → 188α: 6% (α-HO → α-LU+1) 186β → 188β: 6% (β-HO → β-LU+1) 185α → 187α: 6% (α-HO−1 → α-LU) 185β → 187β: 6% (β-HO−1 → β-LU) 185α → 191α: 4% (α-HO−1 → α-LU+4) 185β → 191β: 4% (β-HO−1 → β-LU+4)

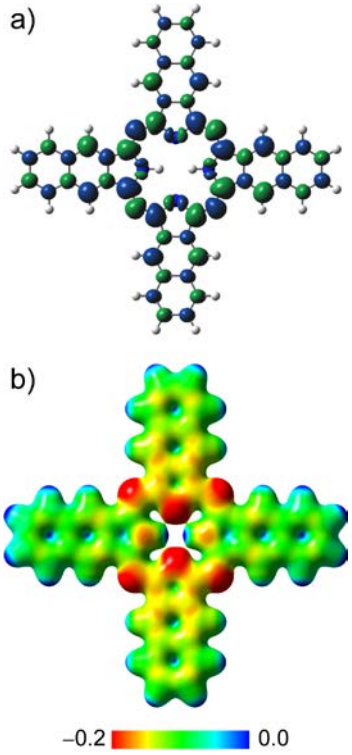

Fig. S11. (a) The isosurface plot for spin density distribution, where the isosurface value is 0.0016 electron/au^3, where the isosurfaces in blue and green denote the positive and negative spin density, respectively, and (b) the electrostatic potential maps on the 0.02 electron/au^3 of electron density surface for the broken symmetry singlet state of C_2-symmetric H_2Nc^{2-} calculated at the UCAM-B3LYP/cc-pVDZ level of theory.

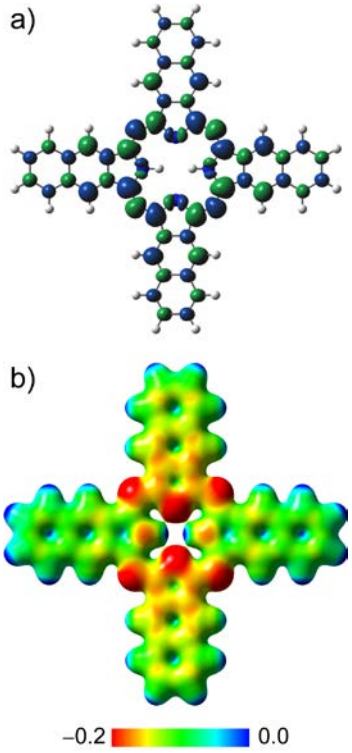

Fig. S12. (a) The isosurface plot for spin density distribution, where the isosurface value is 0.0016 electron/au^3, where the isosurfaces in blue and green denote the positive and negative spin density, respectively, and (b) the electrostatic potential maps on the 0.02 electron/au^3 of electron density surface for the broken symmetry singlet state of C_2-symmetric H_2Nc^{2-} calculated at the UM11/cc-pVDZ level of theory.

References.

1. J. P. Perdew, K. Burke, M. Ernzerhof, *Phys. Rev. Lett.*, **1996**, *77*, 3865–3868.
2. W. J. Stevens, H. Basch, M. Krauss, *J. Chem. Phys.* **1984**, *81*, 6026.
3. D. N. Laikov, *Chem. Phys. Lett.*, **2005**, *416*, 116–120.
4. F. L. Hirshfeld, *Theor. Chim. Acta*, **1977**, *44*, 129–138.
5. T. Yanai, D. Tew, N. Handy, *Chem. Phys. Lett.*, **2004**, *393*, 51–57.
6. R. Peverati, D. G. Truhlar, *J. Phys. Chem. Lett.*, **2011**, *2*, 2810–2817.
7. T. H. Dunning, Jr. *J. Chem. Phys.* **1989**, *90*, 1007–1023.
8. NBO, Version 3.1, E. D. Glendening, A. E. Reed, J. E. Carpenter, F. Weinhold.
9. Gaussian 09, Revision D.01, M. J. Frisch, G. W. Trucks, H. B. Schlegel, G. E. Scuseria, M. A. Robb, J. R. Cheeseman, G. Scalmani, V. Barone, B. Mennucci, G. A. Petersson, H. Nakatsuji, M. Caricato, X. Li, H. P. Hratchian, A. F. Izmaylov, J. Bloino, G. Zheng, J. L. Sonnenberg, M. Hada, M. Ehara, K. Toyota, R. Fukuda, J. Hasegawa, M. Ishida, T. Nakajima, Y. Honda, O. Kitao, H. Nakai, T. Vreven, J. A. Montgomery, Jr., J. E. Peralta, F. Ogliaro, M. Bearpark, J. J. Heyd, E. Brothers, K. N. Kudin, V. N. Staroverov, T. Keith, R. Kobayashi, J. Normand, K. Raghavachari, A. Rendell, J. C. Burant, S. S. Iyengar, J. Tomasi, M. Cossi, N. Rega, J. M. Millam, M. Klene, J. E. Knox, J. B. Cross, V. Bakken, C. Adamo, J. Jaramillo, R. Gomperts, R. E. Stratmann, O. Yazyev, A. J. Austin, R. Cammi, C. Pomelli, J. W. Ochterski, R. L. Martin, K. Morokuma, V. G. Zakrzewski, G. A. Voth, P. Salvador, J. J. Dannenberg, S. Dapprich, A. D. Daniels, O. Farkas, J. B. Foresman, J. V. Ortiz, J. Cioslowski, D. J. Fox, Gaussian, Inc., Wallingford CT, 2013.